USED FUEL DISPOSITION CAMPAIGN

STRUCTURAL SENSITIVITY OF DRY STORAGE CANISTERS

Fuel Cycle Research & Development

Prepared for
U.S. Department of Energy
Used Fuel Disposition Campaign

Nicholas Klymyshyn
Naveen Karri
Harold Adkins
Brady Hanson

Pacific Northwest National Laboratory

September 27, 2013
PNNL-22814
FCRD-UFD-2013-000378

Reviewed by:

PNNL Project Manager

Signature on file

_____

Brady Hanson

EXECUTIVE SUMMARY

This report fulfills the M3 milestone M3FT-13PN0810029 under Work Package FT-13PN081002.

This LS-DYNA modeling study evaluated a generic used nuclear fuel vertical dry storage cask system under tip-over, handling drop, and seismic load cases to determine the sensitivity of the canister containment boundary to these loads. The goal was to quantify the expected failure margins to gain insight into what material changes over the extended storage lifetime could have the most influence on the security of the containment boundary.

It was determined that the tip-over case offers a strong challenge to the containment boundary, and identifies one significant material knowledge gap, the behavior of welded stainless steel joints under high-strain-rate conditions. High strain rates are expected to increase the material's effective yield strength and ultimate strength, and may decrease its ductility. Determining and accounting for this behavior could potentially reverse the model prediction of a containment boundary failure at the canister lid weld. It must be emphasized that this predicted containment failure is an artifact of the generic system modeled. Vendor specific designs analyze for cask tip-over and these analyses are reviewed and approved by the Nuclear Regulatory Commission.

Another location of sensitivity of the containment boundary is the weld between the base plate and the canister shell. Peak stresses at this location predict plastic strains through the whole thickness of the welded material. This makes the base plate weld an important location for material study. This location is also susceptible to high strain rates, and accurately accounting for the material behavior under these conditions could have a significant effect on the predicted performance of the containment boundary.

The handling drop case was largely benign to the containment boundary, with just localized plastic strains predicted on the outer surfaces of wall sections. It would take unusual changes in the handling drop scenario to harm the containment boundary, such as raising the drop height or changing the impact angle.

The seismic load case was derived from the August 23, 2011 earthquake that affected the North Anna power station. The source of the data was a monitoring station near Charlottesville, Virginia, so the ground motion is not an exact match. Stresses on the containment boundary were so low, even from a fatigue standpoint, that the seismic load case is generally not a concern.

Based on this study, it is recommended that high strain rate testing of welded stainless steel test samples be pursued to define the currently unknown material behavior. Additional modeling is recommended to evaluate specific dry storage cask system designs subjected to tip-over loads using a high level of model detail. Additional modeling of the canister interior components (basket, fuel assemblies, etc.) is also recommended, to evaluate the feasibility of fuel retrievability after a tip-over incident. Finally, additional modeling to determine how much degradation a system could undergo and still maintain the integrity of the confinement barrier should be performed.

CONTENTS

FIGURES

TABLES

ACRONYMS

CSCM	cap surface concrete model
DSC	dry storage cask
FEA	finite element analysis
ISFSI	independent spent fuel storage installation
NRC	U.S. Nuclear Regulatory Commission
PT	pseudo tensor
USGS	U.S. Geologic Survey

STRUCTURAL SENSITIVITY OF DRY STORAGE CANISTERS

1. INTRODUCTION

Extended dry storage of used nuclear fuel offers a number of technical challenges. One of the challenges is predicting the behavior of materials over an as-yet undefined length of time, potentially on the scale of hundreds of years. It is expected that time-dependent processes such as creep, oxidation, corrosion, or other phenomena could affect the structural materials that compose the dry storage cask system or its contents. Extensive materials research could be needed to address all of the potential material changes that can happen over an extended service life. This study attempts to identify which material degradation processes are most important to the containment boundary of used nuclear fuel in a hypothetical vertical dry storage cask (DSC) system.

This study performed finite element analysis (FEA) of a generic DSC system subjected to loads anticipated during normal conditions of storage. The purpose was to explore the sensitivity of the used fuel canister to these loads, and to help determine which material degradation mechanisms are most important to the fuel containment boundary. Hypothetical accident conditions were outside the scope of this study, under the assumption that any fuel that experiences an accident will be treated with special care and handling. The focus of this study is on the majority of the used fuel stockpile.

The generic DSC system modeled in this study does not correspond to an existing design. Materials, dimensions, and characteristics were inspired by two different systems that have been licensed by the U.S. Nuclear Regulatory Commission (NRC). Generally, the model was a canister from one vendor within a cask from a different vendor. The goal of this study was to use reasonably realistic dimensions to make general conclusions about DSC behavior, without modeling an existing design in precise detail. Because of this, the results cannot and should not be used to infer the actual expected performance of any existing system under the load cases evaluated. In order to evaluate a system's specific sensitivity to material degradation during extended storage periods, a more design-specific model would need to be constructed and evaluated.

The three load cases chosen for this study included tip-over, handling drop, and seismic response. The tip-over case represents the vertical DSC falling onto its side on the concrete pad. While this could be considered an accident, it is viewed as a design basis event by the NRC rather than a hypothetical accident condition. The handling drop load case represented a canister drop of 12 inches (0.3 m) into the bottom of the DSC, as might happen when the canister is manipulated out of its transfer cask into the vertical storage cask. The seismic response load case represented the cask and pad being subjected to earthquake ground motion. The applied ground motion was derived from the earthquake that affected the North Anna Power Station on August 23, 2011. Note that just as the modeled DSC did not match any vendor's actual design, the seismic models did not attempt to calculate precisely what occurred at the North Anna site.

The model results were analyzed to determine the time-history structural response of the DSC system, with a primary focus on the canister containment boundary. The response of the outer cask system and the structures internal to the canister were also evaluated, as a secondary priority. Each load case offered a transient stress response, so the interest was in the peak stresses or strains occurring over time. Since plastic deformation accumulates and does not relax, that quantity was of particular interest to these kinds of results.

Each loading scenario was first evaluated with a baseline finite element model, using a moderately refined mesh. Certain refinements to the model were then made to explore its sensitivity to certain assumptions, resulting in a baseline results case and a number of additional sensitivity cases. The whole family of results was used to make conclusions regarding the structural response of the system.

Section 2.0 describes the models, loads, and type of results the models provided. Section 3.0 covers the tip-over analyses, Section 4.0 covers the handling drop analyses, and Section 5.0 covers the seismic analyses. Each of the topical sections discusses preliminary model results, final model results, and any additional sensitivity modeling applied to better understand the scenario. Section 6.0 discusses the conclusions that can be drawn from this work, and suggests follow-up analyses. Section 7.0 lists references.

2. CASK MODEL DESCRIPTION

A single cask model forms the basis of all three load cases. Half-symmetry was used to reduce the model size, with a symmetry plane applied along the central axis of the DSC. Figure 2-1 shows the full model in the tip-over load case. The very bottom of the model was a volume of soil. The soil supported a section of the independent spent fuel storage installation (ISFSI) concrete pad. The outermost section of the DSC was concrete, and within that concrete was defined a network of rebar (a). Within the concrete was a steel structure representing the cask liner, base weldment, and lid (b). The canister (c) had a relatively thick base plate and lid connected by a relatively thin cylinder wall. Within the canister were basket supports that ran most of its axial length. The basket (d) was a thin shell structure that formed 16 fuel compartments in this half-symmetry model (32 total). The fuel assemblies were defeatured and represented as blocks of material, with fuel spacers defined at the top (lid) of the canister to take up the extra axial space available (e).

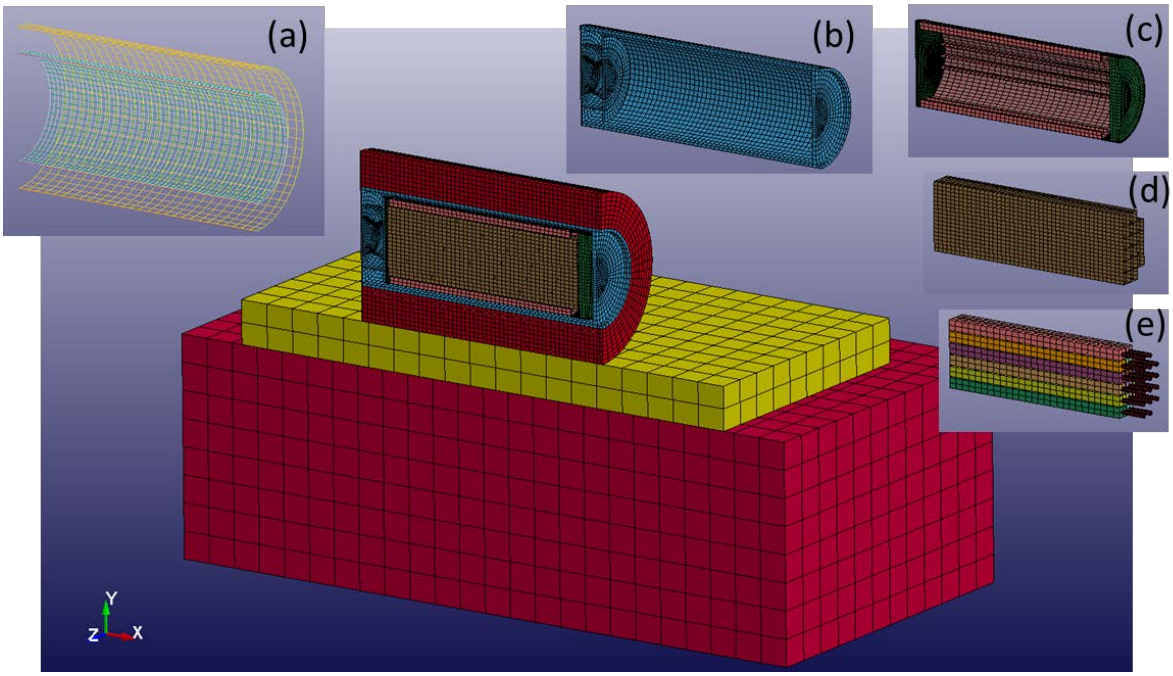

Figure 2-1. DSC Model (Tip-over). (a) Rebar within Concrete Overpack, (b) Steel Cask Liner, Base Weldment, and Lid, (c) Canister with Basket support Rails, (d) Fuel Basket, (e) Fuel Assemblies and Fuel Spacers

2.1 Finite Element Analysis Geometry

This model comprised hexahedral solid elements, shell elements, and beam elements. The LS-DYNA element formulations used as standard in the model were constant stress solid elements, Belytschko-Tsay shell elements, and Hughes-Liu beams with cross section integration (LSTC vol. 1 2012). These represented economical choices for the finite element formulations. In some cases the effect of the choice of formulation was tested with additional analyses. Overall, the standard element formulations were adequate for the analyses.

The mesh density was chosen to provide a reasonable mix of fidelity and computational efficiency. Since the canister was the focus of this study, the goal was to start with a reasonable coarse mesh, and subsequently refine the mesh at specific locations or implement higher order element formulations if necessary in follow-up models. The baseline canister mesh is shown in Figure 2-2. Solid (hexahedral) elements were defined with at least two elements through the wall thickness. The canister shell was modeled with shell elements having at least seven integration points, and the connection to the solids was made using the LS-DYNA constrained-shell-to-solid option, which ensured forces and moments were properly transmitted between the different element types. This treatment significantly reduced the number of elements that would be needed if solid elements were used throughout the shell. The response of the weld regions was of particular interest to this study. From preliminary modeling, the greatest peak stresses and strains were expected to occur in the canister shell wall near the lid in the tip-over load case.

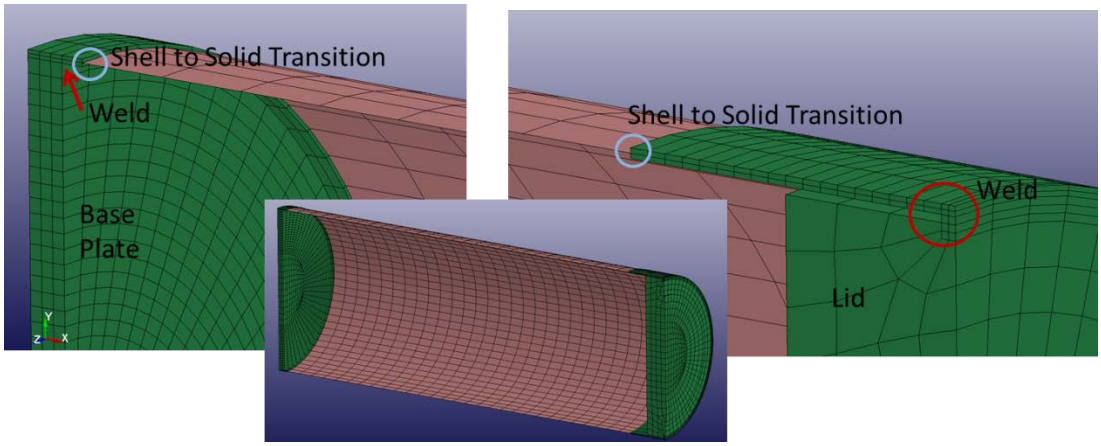

Figure 2-2. Canister Model Details

There were instances in the other components of the system where only a single hexahedral element exists through a wall thickness, but these were restricted to the cask liner (a thick steel wall) and the cask base (also a relatively thick steel structure). In these locations the stress results were not of interest to this study. Their only purpose in the model was to provide a reasonably realistic interaction with the canister. In the tip-over case, the thick steel cask liner is expected to behave largely like a rigid body, and thus did not require a significant number of elements through the thickness. In the handling drop case, the cask base weldment acts something like a spring, an elastic structure that deflects under the impact of the falling canister and ultimately pushes the canister back up with a rebound response. The geometry of the cask base was defeatured to simplify the model; therefore it did not precisely match the existing design. It was reasonable to assume this altered the canister deceleration response to some degree, but since the intent of this study was to not precisely model an existing DSC system, this deviation from the design and the coarse mesh were still adequate for the purpose of this study.

2.2 Boundary Conditions

One key boundary condition was the symmetry plane, which was defined in model space on the Z=0 plane. This choice effectively cut the model size in half and is commonly done in this type of analysis. One of the disadvantages of this approach is that it forces the canister and its contents to remain on the symmetry plane when they actually have some freedom to move out of

the plane if forces during impact become unbalanced. This could conceivably affect the fuel basket behavior and the exact load path through the canister, but these effects are expected to be small. The results did not suggest any need to explore the response with a fully 3D model.

The bottom surface of the soil volume was fixed in space, with nonreflective boundary conditions imposed on the soil periphery. The concrete ISFSI pad was connected to the soil volume with a tied surface-to-surface contact definition, which kept the contacting faces together throughout the analyses. Another option considered in preliminary modeling was to treat the surfaces as sliding, with a relatively high coefficient of friction between them. This option was explored in preliminary modeling and found to have a minimal effect on the results of interest. In the seismic load cases the soil was removed and acceleration time histories were applied directly to the concrete ISFSI pad.

The ISFSI concrete pad to the concrete cask overpack contact was defined as sliding contact with a static and dynamic coefficient of friction of 0.25. This is lower than the value of 0.5 experimentally determined in Shirai et. al (2007), but this was not expected to make a significant difference. In the seismic cases this treatment is expected to allow more relative motion between the DSC and the ISFSI pad than might be realistic. This will be discussed further in the seismic load case discussion.

All sliding contact definitions assumed dynamic and static coefficients of friction of 0.25. Concrete-to-concrete and steel-to-steel coefficients of friction were expected to be higher. This lower value was chosen to ensure the energy dissipated by friction remained within reasonable levels. The primary energy dissipation mechanism in the tip-over case was material deformation, such as crushing concrete and plastically deforming steel. Friction accounted for a non-trivial fraction of total energy dissipation, but most of its contribution was after impact in the rebound phase of the response.

2.3 Materials

The standard model materials are listed in Table 2-1. Steel materials are represented with bilinear elastic-plastic curves with a tangent modulus that is 1 percent of the elastic modulus. This treatment is intended to maximize plastic deformations when they occur and does not fully account for realistic strain hardening. Where sensitivity cases were analyzed with more realistic post-yield behavior, the details were noted in the results discussion. The temperatures these materials represent were relatively low, compared to the maximum design temperature of the DSC systems, which can exceed 400°C (752°F). Higher temperatures tended to lower the yield strength, and this was evaluated with a sensitivity analysis.

Table 2-1. Standard Material Properties

	ASTM A36 Steel (Cask Liner, 100F)	Stainless Steel (Type 304, 200F)[a]	ASTM A615, Grade 60 carbon steel (Rebar)	Soil (Elastic)	Concrete (discussed below)
Density	7860 kg/m3	8050 kg/m3	7860 kg/m3	2560 kg/m3	2563 kg/m3
Poisson's Ratio	0.31	0.31	0.31	0.45	.22
Modulus of elasticity	200 GPa	190 GPa	200 GPa	414 MPa	-
Yield Strength	248MPa	172MPa	414 MPa	-	-
Tangent Modulus	2 GPa	1.9 GPa	2 GPa	-	-

[a] ASME code values (ASME 2011)

The concrete was evaluated with two nonlinear material models, the pseudo tensor (PT) and continuous surface cap model (CSCM), available in LS-DYNA. These concrete models are described in detail in LSTC vol. 2 (2012), and additional information is available in Murray (2007). The PT material formulation has a long history of use for this type of analysis, but the CSCM was more recently developed and had been demonstrated in testing by Murray et. al (2006) to provide a more accurate prediction of concrete damage in highway structures. The PT model was considered the baseline material, with the CSCM used in sensitivity studies. The source of the PT model input parameters was Witte et. al (1998) and the LS-DYNA code for implementing it is shown in Figure 2-3, with the material inputs above and the corresponding equation of state inputs below. The CSCM concrete was defined to have equivalent crush strength and the code for implementing it is listed in Figure 2-4. Both concrete material models represent the same basic composition of concrete, with the difference in behavior caused by the treatment of the damage.

mid	ro	g	pr	-	-	-	-
1	2563	1.03E+10	0.22	-	-	-	-
sigf	a0	a1	a2	a0f	a1f	b1	per
5.9984E+06	1.3790E+07	4.1800E-01	1.2110E-08	0.0000E+00	3.8500E-01	0.0000E+00	0.0000E+00
er	prr	sigy	etan	lcp	lcr	-	-
0.0	0.0	0.0	0.0	0	0	-	-
x1	x2	x3	x4	x5	x6	x7	x8
0	9.40E-04	0.00296	0.00837	0.01317	0.0234	0.04034	1
x9	x10	x11	x12	x13	x14	x15	x16
0.0	0.0	0.0	0.0	0.0	0.0	0.0	0.0
ys1	ys2	ys3	ys4	ys5	ys6	ys7	ys8
0.00000	0.28900	0.46500	0.62900	0.77400	0.89300	1.00000	1.00000
ys9	ys10	ys11	ys12	ys13	ys14	ys15	ys16
0.0	0.0	0.0	0.0	0.0	0.0	0.0	0.0

eosid	gama	e0	vo	-
1	0	0	0	-
ev1	ev2	ev3	ev4	ev5
0.000E+00	-6.000E-03	-7.500E-03	-1.000E-02	-1.200E-02
ev6	ev7	ev8	ev9	ev10
-2.000E-02	-3.800E-02	-6.000E-02	-7.550E-02	-9.700E-02
c1	c2	c3	c4	c5
0.000E+00	3.172E+07	3.723E+07	4.275E+07	4.551E+07
c6	c7	c8	c9	c10
5.378E+07	6.895E+07	8.687E+07	1.034E+08	1.289E+08
t1	t2	t3	t4	t5
0.000E+00	0.000E+00	0.000E+00	0.000E+00	0.000E+00
t6	t7	t8	t9	t10
0.000E+00	0.000E+00	0.000E+00	0.000E+00	0.000E+00
k1	k2	k3	k4	k5
4.826E+09	4.826E+09	4.826E+09	4.826E+09	4.826E+09
k6	k7	k8	k9	k10
4.826E+09	4.826E+09	4.826E+09	4.826E+09	4.826E+09

Figure 2-3. Pseudo Tensor Concrete Model Data

mid	ro	nplot	incre	irate	erode	recov	itretrc
1	2563	1	0.00	0	1.1	0.00	0
pred	-	-	-	-	-	-	-
0.00	-	-	-	-	-	-	-
fpc	dagg	units	-	-	-	-	-
2.80E+07	0.019	4	-	-	-	-	-

Figure 2-4. CSCM Concrete Model Data

2.4 Loads

Gravity was included in all models. The seismic models were initialized with nodal deflections caused by gravity. The nodal deflections were calculated in a transient preload analysis of the as-built model, applying gravity acceleration and a high mass damping value to determine how

much the system settles. This avoided the transient effect of applying gravity as a step load at the first timestep.

The tip-over and handling drop cases were primarily loaded with initial velocities. The tip-over case used an angular velocity while the handling drop was a translational velocity. Both initial velocity loads were determined using conservation of energy methods for rigid body motion.

The primary loads of the seismic case were vertical and horizontal acceleration histories applied to the bottom nodes of the concrete pad. These motions were based on recorded earthquake data associated with the earthquake that affected the North Anna power station in August 2011. The construction of the earthquake loads from raw data is discussed in Section 5.1.

2.5 Results

The focus of this study is on the stress and strain response of the canister containment boundary, the baseplate, canister shell, lid, and the welds that secure the components together. In the context of extended long term storage of used fuel, the interest is in identifying the most challenged aspects of the containment boundary. Peak instantaneous stresses and through-wall average stresses are collected at many locations, including the highest stress regions for every component. The magnitude of stresses can be used to gauge how much of a safety margin exists in the modeled scenario. Since these are not intended to be precise representations of actual DSC designs these safety margins offer a general sense for where the critical locations are, but do not reflect a performance expectation for existing designs.

The explicit finite element method calculates results at a relatively small time step, so results must be saved to the hard disk at a much lower frequency to avoid filling up the system. Overall stress results were preserved at a reasonable frequency. For the tip-over and handling cases one solution state is written every millisecond. For the longer running seismic cases results were written every 10 milliseconds.

The dynamic response of the DSC components was a side interest, particularly the dynamic loads applied to the fuel assemblies. Fuel retrievability is a significant interest to the used fuel disposition community, which was not studied in this body of work, but is planned for future work. Pacific Northwest National Laboratory (PNNL) has the capability to model full fuel assemblies subjected to dynamic loads, as in Klymyshyn et. al (2013).

3. TIP-OVER LOAD CASE

The preliminary modeling work for this study first focused on capturing the proper tip-over physics, with the DSC falling over and impacting a section of concrete pad with soil below. This involved an investigation of the best way to model concrete in LS-DYNA. It was eventually decided to use two separate concrete material formulations on the basis that one (pseudo tensor) has been widely used in the nuclear industry, and that a second (CSCM) has a better ability to model damage mechanisms in concrete, as demonstrated through recent testing on highway structures (Murray et. al 2006). Since the degradation of concrete is a potential issue of interest, both types of concrete were run for comparison. Preliminary modeling showed a difference in the dynamic response during tip-over and in the concrete damage patterns. In the final analyses, the pseudo tensor material model is considered the baseline material and the CSCM material was used in sensitivity studies.

A second focus of the preliminary modeling was to determine where the regions of greatest stress occurred to guide the formulation of a more detailed and sophisticated model of the canister. In the preliminary models, the canister was simply represented with brick (hexahedral) elements with a coarse mesh and just one element through the canister wall thickness. The stress results showed that high stresses developed in the canister shell wall where it transitioned to the base plate and lid, and at other places in the canister shell wall. This preliminary modeling work led to the baseline canister representation shown in Figure 2-2. Higher mesh densities are considered in additional sensitivity studies.

3.1 Baseline Tip-over Case

The tip-over scenario is modeled beginning at the moment of impact of the top edge of the cask with the ISFSI pad. The time it takes for the cask to rotate from a vertical to a horizontal orientation is not modeled. The applied initial rotational velocity was 1.51 radians/s, which was derived through conservation of energy applied to the change in height of the cask center of mass from the vertical to horizontal position. The model was solved to a time of 100 ms (microseconds, 0.001 s), which covers the initial impact and ends with the cask system having a positive rebound velocity. Full settling is expected to take up to two seconds, which would increase the run time by a factor of 20. A single long-running case is solved as a sensitivity study.

The rigid body acceleration response of the cask system center of mass and one fuel assembly is plotted in Figure 3-1. The cask system curve represents the sum-total center of mass of the DSC system, including every component of the model except the ISFSI concrete pad and the volume of soil below it. The fuel assembly curve tracks the center of mass of the centrally located fuel assembly closest to the point of impact. The cask system as a whole experiences a peak deceleration of about 2.9 g, over a pulse duration of about 40 ms. The fuel assembly can be seen to have a much livelier deceleration, with a brief peak up to 161 g, with multiple pulse durations below 10 ms in duration. The fuel assembly response is not the focus of this study, but this acceleration history result raises the question of whether or not this type of deceleration loading might damage the fuel assembly and affect its retrievability, especially if material properties degrade over extended storage. Examination of the fuel assembly and cladding response is planned for future work.

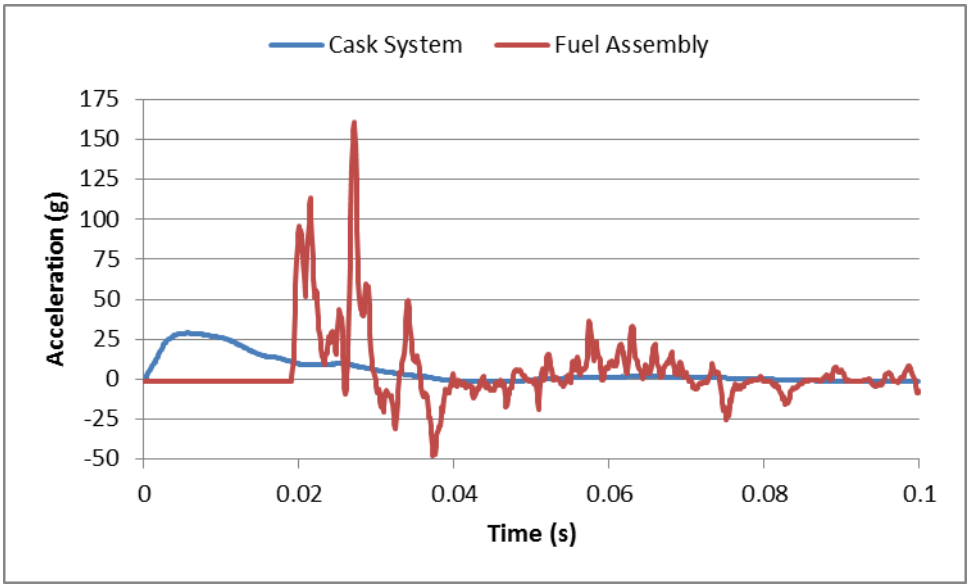

Figure 3-1. Vertical Acceleration Response to Tip-over

The maximum plastic deformation accumulated in the canister structure occurs at the edge of the shell wall that makes the initial contact with the cask liner. The region of interest is plotted in Figure 3-2, with letters to identify the various components. The components are described as follows.

(a) ISFSI concrete pad, which sits on top of a volume of soil, and is not visible in the figure

(b) Concrete cask, which is reinforced with rebar

(c) Steel cask liner includes a lid and base structure. All of the liner, lid, and base components are modeled with a coarse mesh because they are not a focus of this study.

(d) Combined lid, weld, and canister shell structure. A full penetration weld acts to seal the canister, and this is modeled as if the lid and canister shell were one continuous material. A radial gap exists below the weld, between the outer diameter of the lid and the inner diameter of the canister shell. This is a realistic feature, not an overly conservative one.

(e) Points to the shell element representation of the canister shell wall. The shell elements connect to the brick elements of (d) through a special shell-to-solid connection feature in LS-DYNA. The constraint definition properly transfers loads across the interface.

(f) Basket contact rails are simply represented as solid elements rather than the more complicated plate structures that they are in some canister designs. Their only purpose is to transfer forces from the basket to the canister wall. In this case they are expected to cause conservatively high stresses in the canister shell because they are stiffer than would normally be expected.

(g) Fuel basket shell, provides 16 fuel compartments in this half-symmetry model. Within each compartment is a solid block of material to represent the fuel assemblies.

(h) Fuel spacers, one for each fuel compartment, which take up the extra room available at the top of the canister.

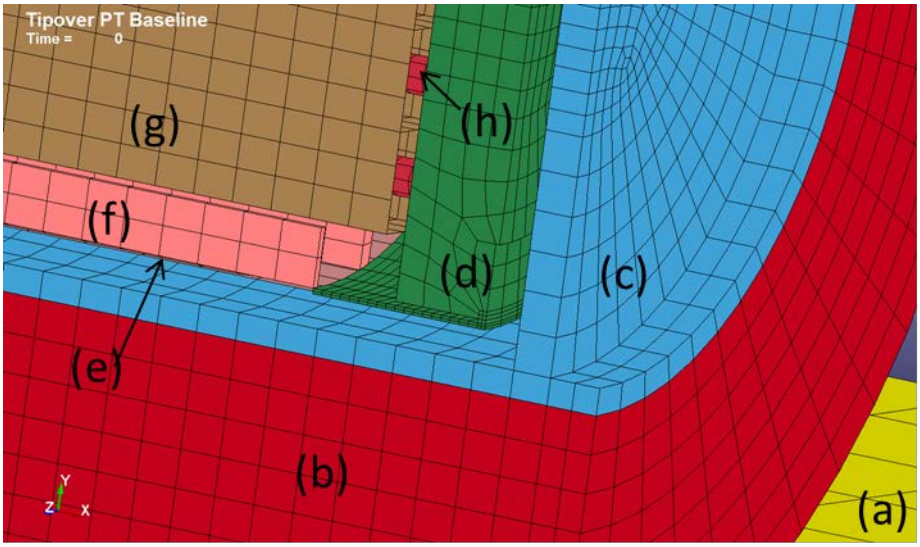

Figure 3-2. Model Components: (a) Concrete Pad, (b) Concrete Cask, (c) Steel Liner, Base, and Closure, (d) Canister Lid, Weld Region, and Portion of Canister Shell, (e) Canister Shell, (f) Fuel Basket Support Rails, (g) Fuel Basket, (h) Fuel Assembly Spacers

Figure 3-3 shows the same region at four moments in the solution history, to illustrate the gaps between components, local deformations, and rebound. Time (a), 0 ms, is the starting condition. In this case a gap of 3 inches (76.2 mm) exists between the canister and the cask liner. This gap size results from the decision to construct a model with mixed features rather than match an existing DSC system. The gap is arguably unrealistic, and the effect of this gap was addressed with a sensitivity study in Section 3.5. At time (b), 16 ms, the deformation of the canister shell near the weld is apparent. At time (c), 32 ms, the fuel basket has started to deform around the solid support rails. With realistic rails and more detailed basket the deformation might not be so great. At time (d), 100 ms, the end of the analysis, the canister has rebounded significantly from the cask.

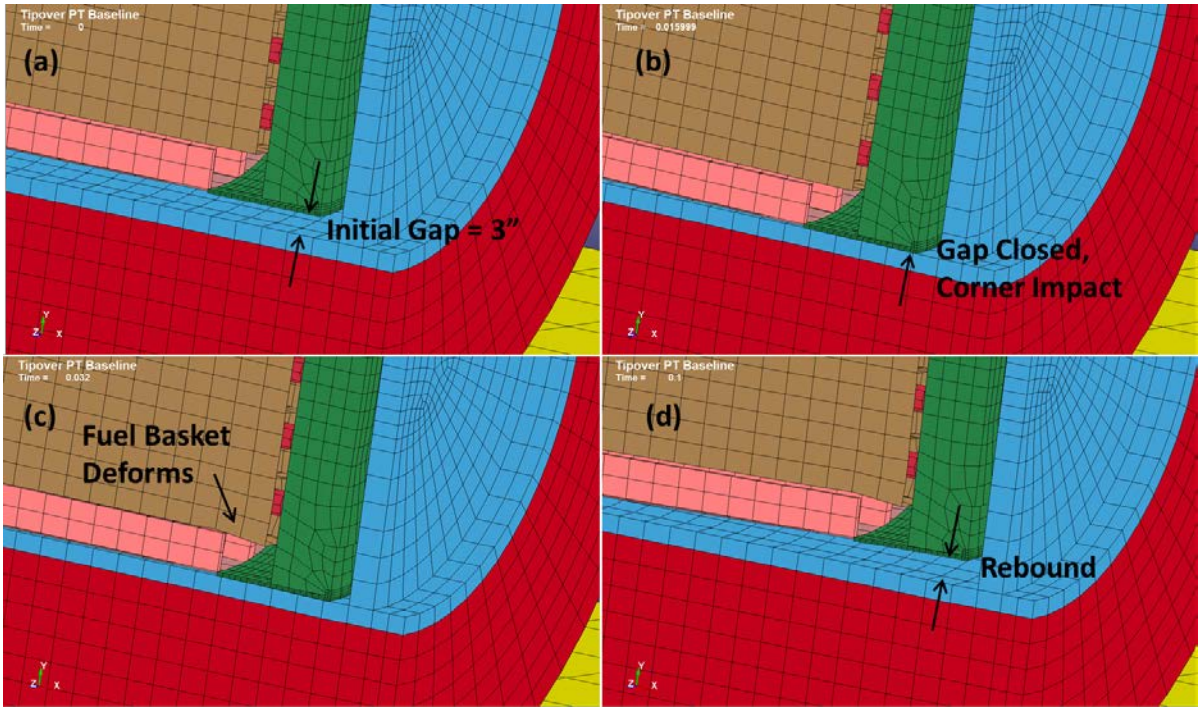

Figure 3-3. Tip-over Response History: (a) 0 ms, (b) 16 ms, (c) 32 ms, (d) 100 ms

As Figure 3-4 shows, the predicted plastic deformation of the cask lid region is significant. The upper cask shell and weld region experience through-wall plastic strains. The plastic strain region extends around the circumference through a number of elements and radially through a number of elements into the coarse mesh region of the lid. Though the mesh density is limited in its refinement, the fact that the plastic strain region crosses a number of elements suggests that the development of plastic strains in the weld region is a credible general conclusion. A finer mesh density is needed to better estimate the stresses and strains spatially through the region. A sensitivity study with a higher mesh density in that region was performed to more precisely quantify the stresses and strains, as detailed in Section 3.3.

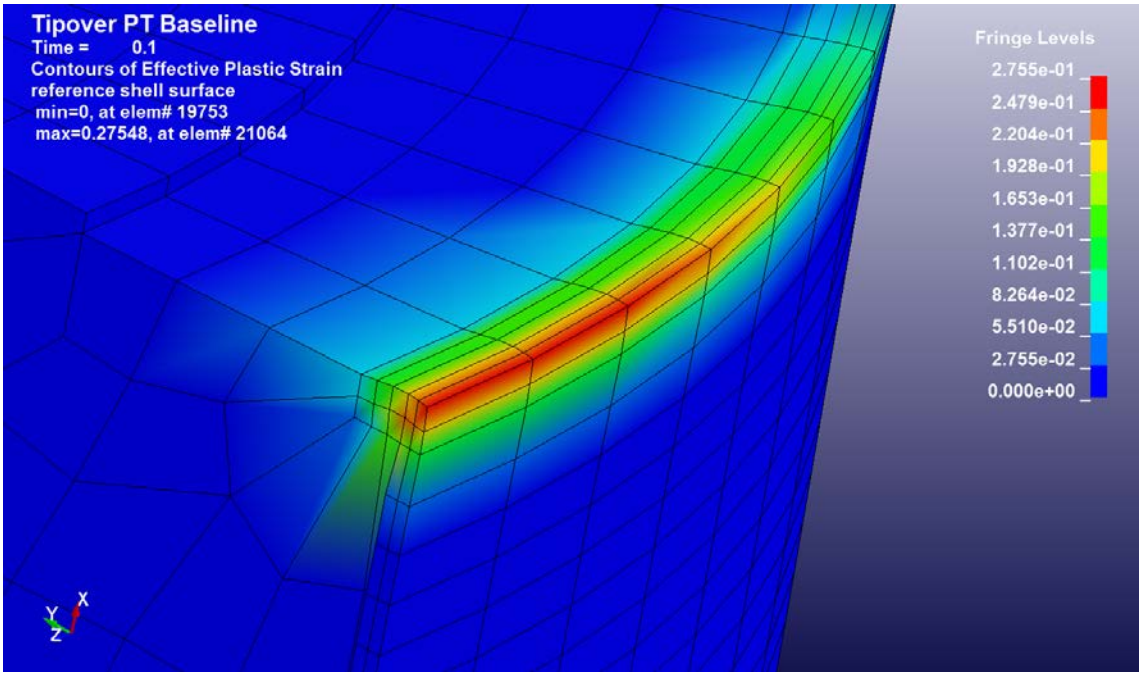

Figure 3-4. Plastic Strain in Canister Lid Weld Region

The baseplate also experiences some plastic strain in a few locations. Figure 3-5 shows the baseplate from two angles. Contours are the equivalent plastic strain, with a peak of 0.0566 displayed. The most significant strain region is near the point of impact with the cask liner (near the bottom of the figure). As in the lid weld region, the fact that that the plastic strains cross into so many elements, and through the baseplate wall thickness, indicates a major trend. The magnitude of the plastic strains is much lower than the lid weld region, less than 0.03 m/m equivalent plastic strain, but this is still indicative of a broad region of material loaded above its yield strength.

Another interesting feature of this plastic strain region is that it starts to develop at 35 ms, which is distinctly after the impact at the lid end. This is physically reasonable, given the gap size and the fact that the initial velocity load was a rotational velocity. From the general dynamic response of the model, the lid end starts to impact at about 15 ms, achieving maximum plastic strains at about 20 ms. The baseplate end starts to impact at about 25 ms, and reaches maximum plastic strains about 40 ms.

The peak stress concentrations on the inside face of the baseplate appear to be because of interaction with the basket corner and a fuel assembly. The basket and fuel assemblies were highly defeatured, so the impact loads that cause the high plastic strain are questionable and the predicted value of the plastic strain is questionable. But this result suggests the possibility that the baseplate could have significant loading applied to it by the fuel assembly payload. The fuel assembly axial accelerations are predicted to exceed 40 g, and this would translate into an impact force against either the base plate or lid. This is for a tip-over scenario, where a strong axial load was not expected.

The final locations of interest on the baseplate are the weld regions around its circumference where the shell is welded to the base. Through-wall plastic strains of some magnitude are

expected all around the baseplate weld region. The maximum occurs at the bottom end point of impact, near the broad plastic strain region. This was investigated more closely in a sensitivity study that implements more realistic strain hardening, as detailed in Section 3.4.

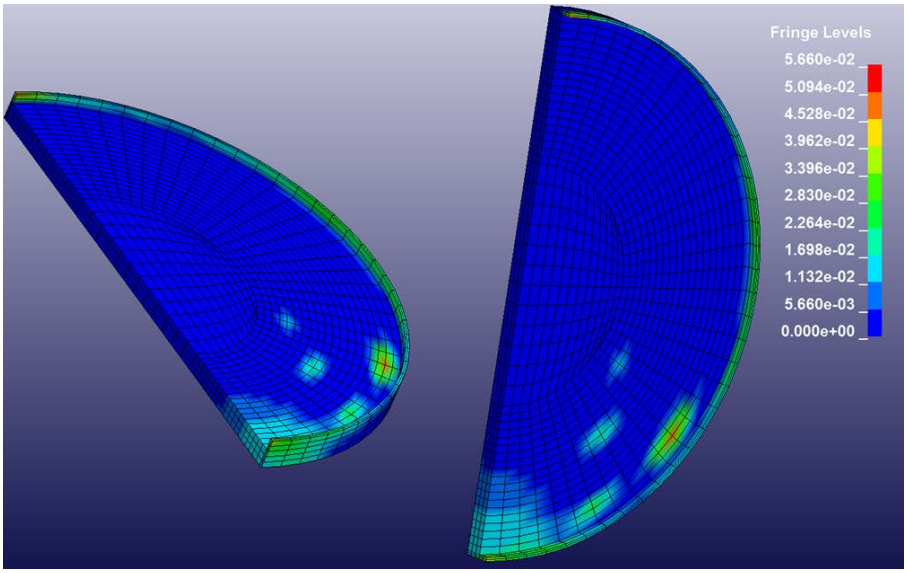

Figure 3-5. Baseplate Plastic Strains, from Two View Angles

3.2 Sensitivity Study: Double Precision

The LS-DYNA code offers two standard executable types, for single and double precision calculations. Single and double refer to the computer number formats used in the calculation, the difference being the number of significant digits in the floating point numbers. It is not easy to predict when models require double precision, which can increase the run time significantly, so standard practice is to calculate the model results with both solvers and compare them.

The baseline tip-over model was run with the double precision solver, and the difference in results was found to be insignificant for the purpose of this study. The most important elements in this case are the lid weld region elements, where significant plastic strains are predicted. Element 21051 is located in the weld region adjacent to the center line at the top of the canister. The plastic strain history of this element is plotted in Figure 3-6. The two lines nearly overlap, with a difference in the post-impact regime of less than 2 percent.

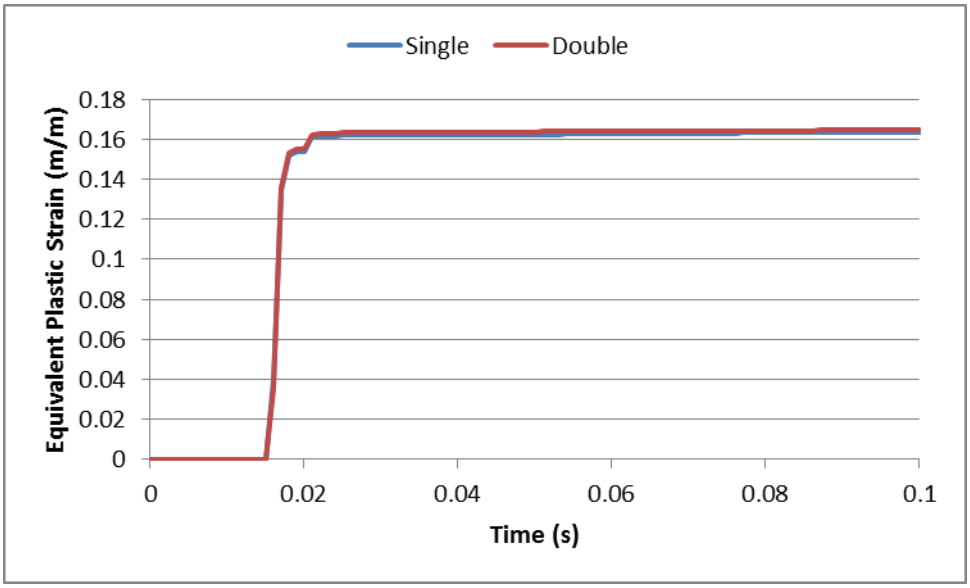

Figure 3-6: Comparative Plastic Strain in Element #21051

An example of more visible difference between single and double precision can be seen in the fuel assembly acceleration responses. The same fuel assembly acceleration response plotted in Figure 3-1. V is plotted as the single curve in Figure 3-7. . The double curve is the double precision response of the same fuel assembly. The visible difference might be a consideration for analyses of the fuel response, but in this case it is outside the scope of this study.

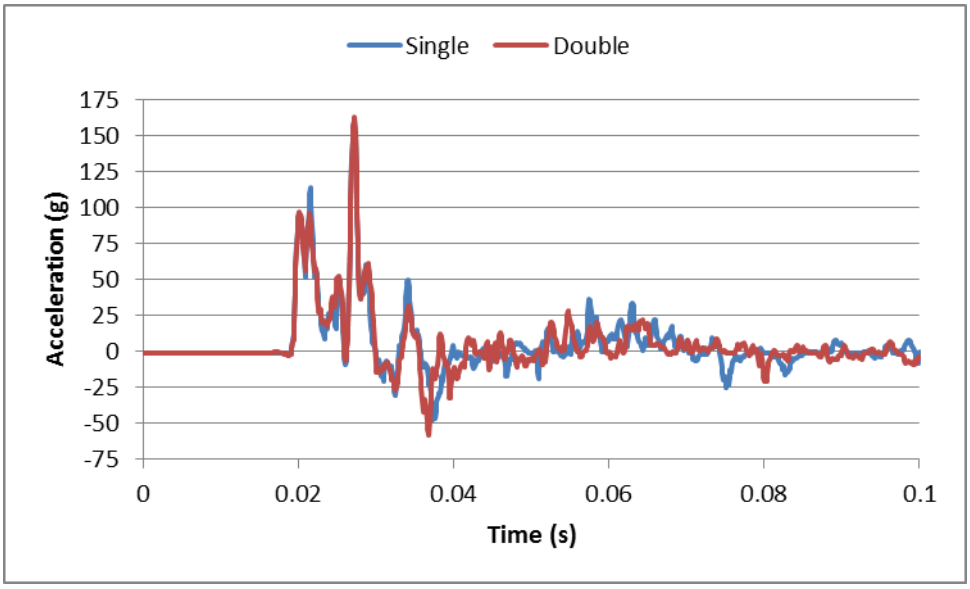

Figure 3-7. Fuel Assembly Acceleration, Single and Double Precision Solvers

It is concluded from this sensitivity study that double precision is not necessary for this study because it has a limited influence on the results of interest. For the seismic cases, which calculate results for tens of seconds, taking multiple days of computer time, solving in double precision mode was not attempted. In the shorter duration runs, some additional exploration of

double precision was made, but all results in this report were calculated using single precision unless noted otherwise.

3.3 Sensitivity Study: Increased Mesh Density

In this case the baseline model was modified to increase the mesh density specifically in the lid weld region. The number of elements around the canister circumference was doubled. The number of elements through the cross section in the upper canister shell and lid region was increased to four, and the transition to larger elements in the lid was smoothed. The key changes to the lid weld region mesh are visible in the deformed plastic strain plots, Figure 3-8 and Figure 3-9. The higher mesh density gives more resolution to the contours and better defines the extent of the plastic strain zone. The maximum plastic strain increased to about 34 percent from about 28 percent in the baseline case, so the difference is not extreme. Generally, the same structural response is predicted in both cases, with the higher mesh density case providing a higher level of confidence in the stress and strain results.

The baseplate region had a similar response to the baseline case, but the only change to the mesh was the doubling of elements around the circumference. The pattern of localized stresses attributed to interaction with the fuel assemblies and basket changed, as shown in Figure 3-10. As discussed in the baseline case results, the defeatured fuel assemblies and basket made the localized peak strains on the inside face of the baseplate questionable. More detailed modeling of the canister interior would be needed to explore this phenomenon further.

The magnitudes of stresses are noted in Table 3-1. Peak stresses are the element maximums. The through-wall stresses are defined by selecting a row of solid elements to define the path through the cross section, plotting the elements' von Mises stress over time, then averaging the stress time histories to find a maximum instantaneous through-wall stress. For shell elements, peak and average shell stress were directly available from the results. Note that the yield strength was 148 MPa, so every stress value reported in Table 3-1 is in the plastic strain range.

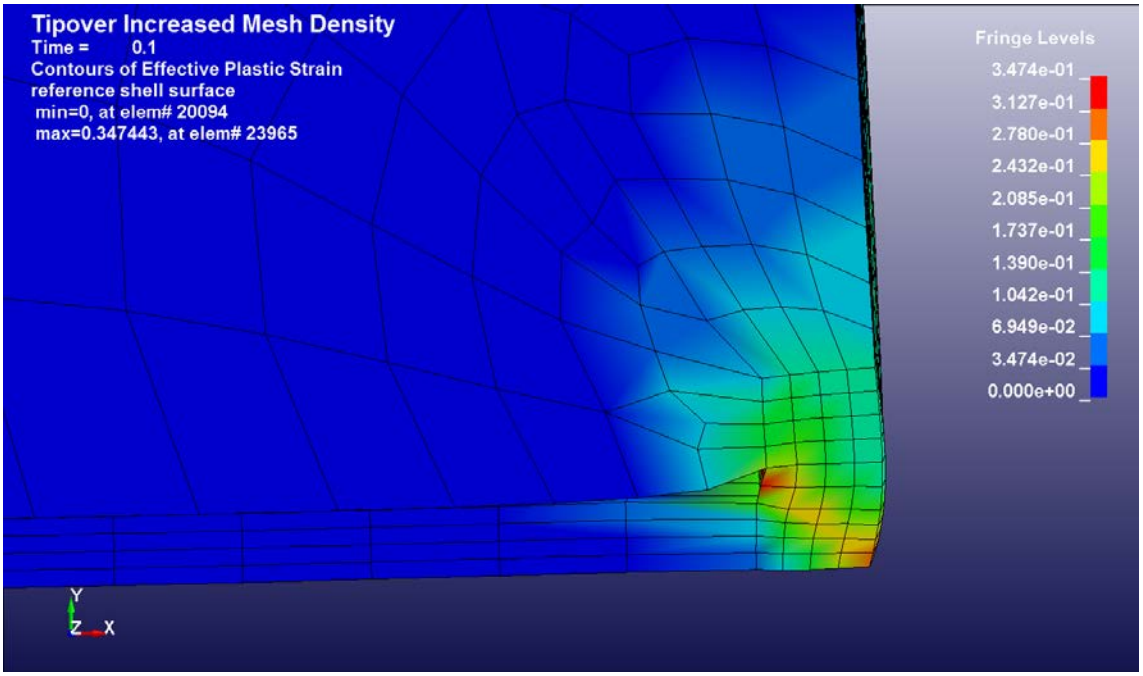

Figure 3-8. Lid Weld Region Plastic Strains, Side View

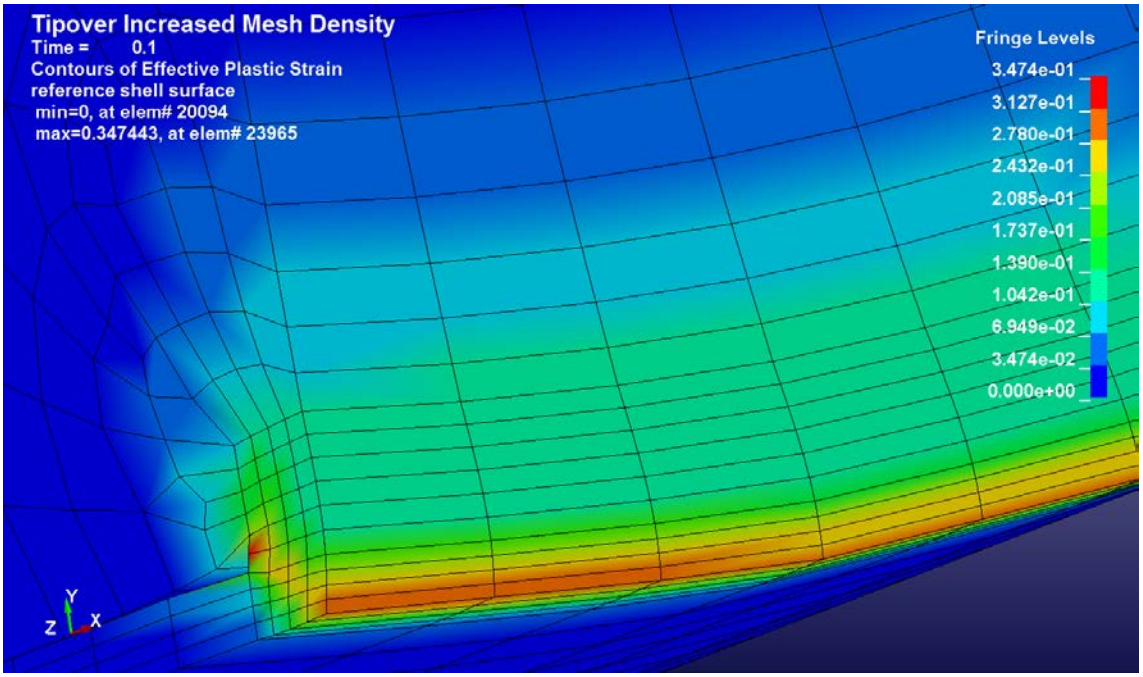

Figure 3-9: Lid Weld Region Plastic Strains, Top View

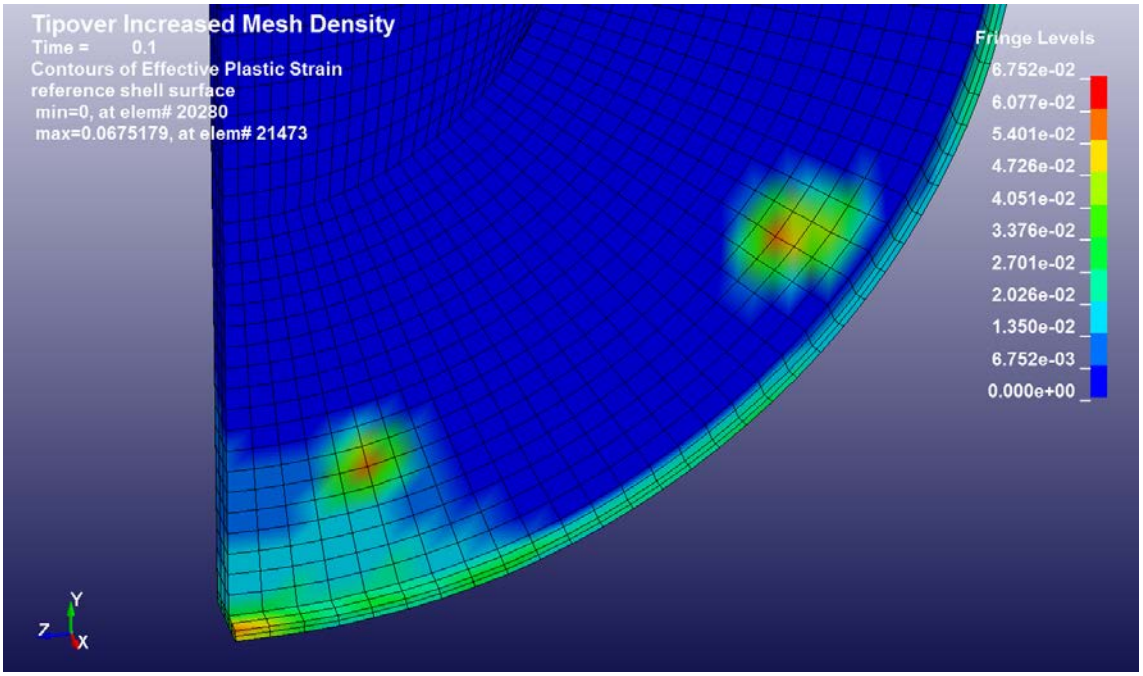

Figure 3-10. Baseplate Plastic Strains

Table 3-1. Tip-over Stress Summary

Location	Peak	Through-wall
Canister Lid Weld	787	594
Canister Shell Wall Maximum	272	238
(Near Lid Weld)	226	208
(In Shell Elements)	272	238
(In Shell Elements Connected to Basket Rails)	199	172
(In Shell Elements Away from Geometric Discontinuities)	171	159
Base Plate Shell Weld	222	210
Base Plate Through Thickness	185	173

The canister lid weld material reached the highest stress and experienced the most plastic strain. The through-wall stress exceeded the material ultimate strength, so these results challenged the integrity of the containment boundary for the hypothetical DSC design modeled in this study. The effect of the bilinear plastic material model is explored in the next section.

One point worth noting on the lid weld response is the rate at which the plastic strains were accumulated. The maximum plastic strain rate, determined as the time derivative of the plastic strain history curve, peaks at 151 m/m/s. For a period of about 4 ms, the strain rate of the maximum element was above 20 m/m/s. Typical strain rates applied during testing are orders of magnitude lower. This will also be discussed more in the next section.

3.4 Sensitivity Study: Multilinear Plastic Material

The key material for this study is the stainless steel of the canister baseplate, shell, and lid. In vendor designs, this material can be defined as Alloy X, which means it can be constructed from a number of specific compositions of stainless steel. In the baseline case, the material values came from ASME (2011) for SA-240, 304L, UNS No. S30403 Plate for temperatures not exceeding 200°F. The yield strength represents a minimum requirement, not an expected value. As stated previously, the post-yield tangent modulus was artificially constructed to be 1 percent of the elastic modulus. Actual material behavior is expected to be different, and could result in less accumulated plastic strain when subjected to the same loads. Accumulated plastic strain is important because one potential measure of failure is exceeding the ductility limit, which is determined experimentally and is expressed as percent-elongation. The calculated plastic strains of the baseline case are up to 27 percent, which is high. This value is within the expected elongation range of annealed 304 and 316 stainless steels, but could be excessive depending on the amount of cold work.

A number of unknowns make it difficult to assign more realistic elastic-plastic behavior to the canister stainless steel. First, the chemical composition of the material can vary from within a family of stainless steel. They are expected to have similar post-yield behaviors, but the difference in chemical composition may be relevant for potential material degradation studies. Second, the temperature at the time of tip-over is important because it affects the yield strength and post-yield behavior. Finally, the amount of cold work in the material and the potential localized effect of the welding process would affect the material yield strength and post-yield behavior.

Another issue associated with the canister stainless steel is the fact that strain rate can affect the material behavior. This is a known material phenomenon, but is not commonly considered in standard structural models. In impact models like the tip-over case, strain rate effects can have an important influence on the accumulated plastic strain.

Considering the baseline response, it is also necessary to define failure criteria for the material. Since the basis of the stainless steel material properties was the ASME code, using the minimum material strength defined by ASME is appropriate. For the baseline material the tensile strength is 482.6 MPa, which in the bilinear material model corresponds to a plastic strain of 18 percent. With this interpretation of the material behavior and limits, the baseline case predicts a failure of the containment boundary because the minimum tensile strength is exceeded through the thickness of the weld region. This conclusion is driven by the conservative model assumptions, and does not necessarily represent the performance of actual DSC systems during a tip-over event. One of the reasons to consider a different material model in this study is that the realistic yield strength and post-yield behavior of the stainless steel is expected to differ from the baseline model.

An alternate multilinear stress-strain curve was constructed using literature sources to define a more realistic shape. AK Steel (2007) lists the typical room temperature strength of its 304L steel as 241 MPa yield strength and 586 MPa ultimate strength. These values are used as the basis of a Ramberg Osgood formulation for the stress strain curve, as described in Mil-HBK-5J (DOD 2003). From MIL-HBK-5J, the adjustment from room temperature to 200°F causes about

an 80 percent reduction in yield and ultimate strength in annealed material. Using the temperature-reduced strength values and a Ramberg-Osgood parameter of 5, the multilinear stress strain relationship in Figure 3-11 was created. In the figure, the baseline stress-strain curve is plotted for comparison. The diamond shaped symbols identify the ultimate strength values and the triangle shapes identify the maximum predicted stress/strain in the corresponding model.

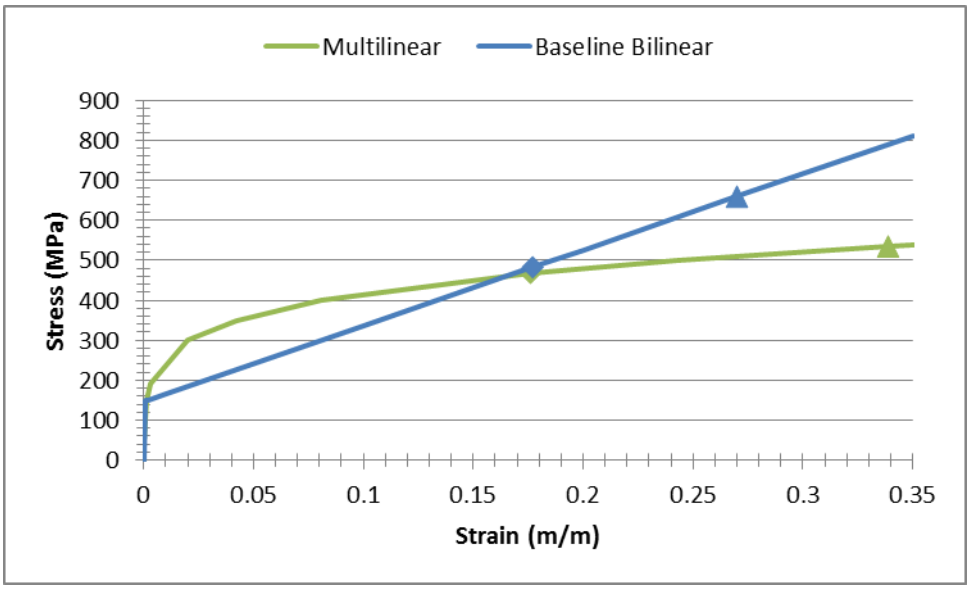

Figure 3-11: Stress-Strain Relationship in Multilinear and Bilinear Models

The results show a very similar response to the baseline case, with the difference being the values of stresses and strains in the post-yield regime because of the differing stress-strain relationship. In an impact scenario like this, the driving phenomenon is the transfer of energy into the structure. The translation of impact energy into deformation energy causes material deformation, as elastic and plastic strain, and altering the stress-strain relationships can have a nonlinear effect on the energy dissipation paths. In this case, the different material formulations do not lead to vastly different responses of the system. Regions of high plastic strain remain regions of high plastic strain. Regions of lower plastic strain remain regions of lower plastic strain. While they are qualitatively the same, the quantitative stress and strain values are affected.

In the baseplate region, Figure 3-12, plastic strains are generally lower than the baseline case. In the lid weld region, Figure 3-13, the plastic strains are higher than the baseline case. As can be seen in Figure 3-11, the transition point between the two curves is a total strain of about 17 percent, which is close to the ultimate strength in both cases. If we consider the ultimate strength to be the material failure limit, both curves indicate failure at nearly the same stress-strain point, though the behavior before and after that point does not match. Since no major changes in response occur, the baseline model bilinear curve is a reasonable representation of the material behavior up to the ultimate strength and slightly beyond, but the calculated stress and strain values from the model outside the elastic range should be treated as an estimate.

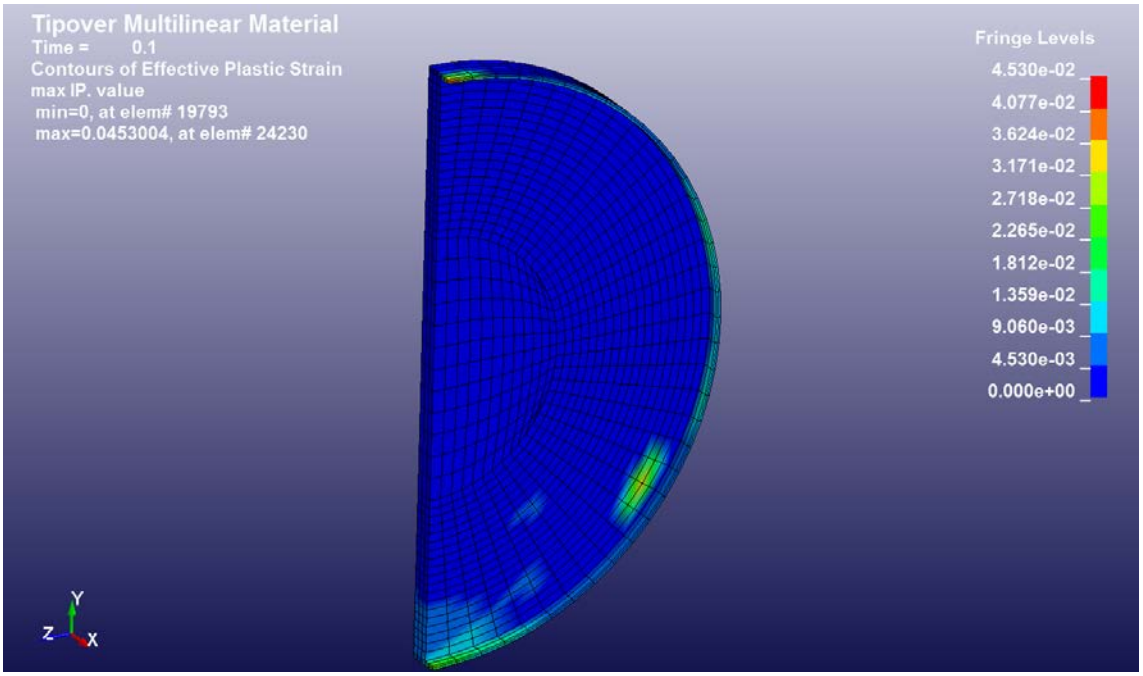

Figure 3-12. Baseplate Plastic Strains with Multilinear Material Model

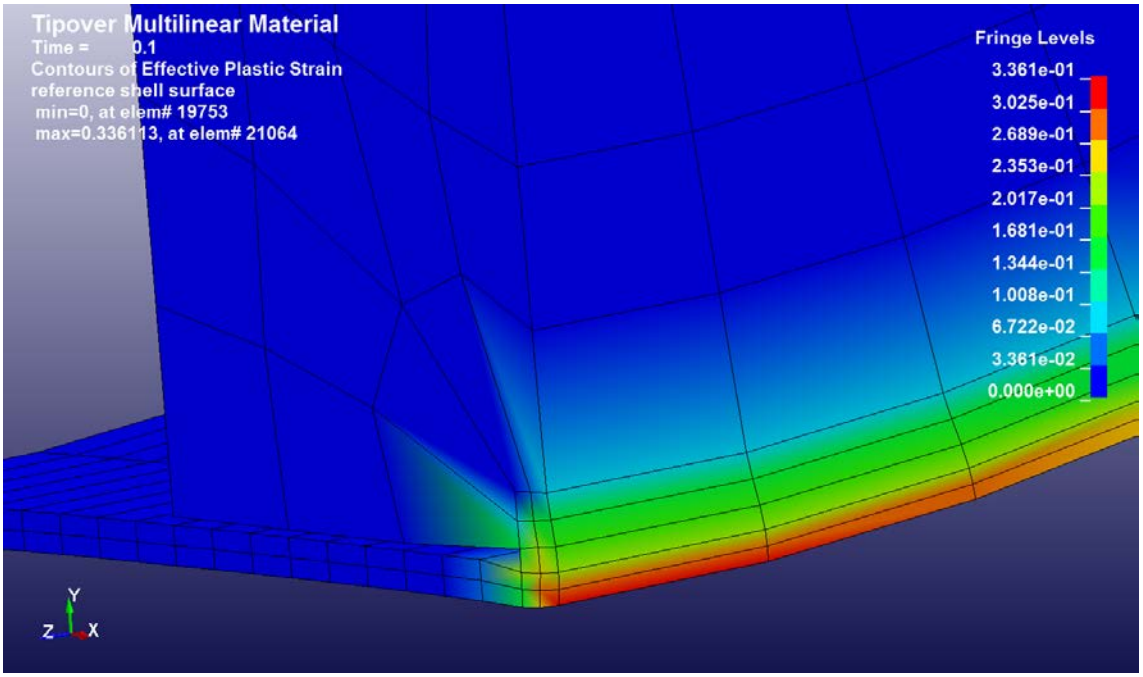

Figure 3-13. Lid Weld Region Plastic Strain with Multilinear Material Model

With the multilinear material model, the lid weld material still experiences considerable plastic strains over a short duration of time. Typical material strengths are determined at relatively slow strain rates. High strain rates can lead to higher yield strength and lower ductility (elongation to failure). These time sensitive material behavior characteristics can be included in this type of impact analysis, but material data to cover the behavior at the anticipated strain rates are needed. The peak plastic strain rate noted in the increased mesh density case was 151 m/m/s. In the

multilinear material model case, the peak strain reaches 127 m/m/s. While this value is somewhat less, it remains in the same order of magnitude and occurs over a similar duration. The lid weld material section has a peak stress of 521 MPa and a through-wall stress of 498 MPa, which are both above the 467 MPa ultimate strength limit, which is based on traditional slow strain-rate testing. It is possible that the material might not actually fail in this scenario, because of an effective increase in strength from the high strain rate. The material might still fail because of reduced ductility at high strain rates. More information on the material behavior is needed to determine the proper material failure criteria. The best that can be concluded at this point is that the lid weld region of this hypothetical DSC design is expected to experience severe stresses and strains in this tip-over loading scenario, beyond its established tensile strength.

It must be emphasized that this predicted containment failure is an artifact of the generic system modeled. Vendor specific designs analyze for cask tip-over and these analyses are reviewed and approved by the NRC and do not result in failure. Still, this generic model demonstrates the sensitivities and importance of understanding the materials, dimensions, and phenomena involved. Based on this study, it is recommended that high strain rate testing of welded stainless steel test samples be pursued to define the currently unknown material behavior.

3.5 Sensitivity Study: In-Cask Channels

As noted previously, the generic DSC system used in this study does not correspond to any existing DSC design. Certain features of the model were drawn from two different systems and mixed together to avoid the possibility that the results could be extrapolated to make performance judgments about existing systems. Unfortunately, this approach led to a hypothetical design that does not adequately withstand the tip-over load case. Because tip-over is a design basis event, any system certified by NRC can be expected to withstand a tip-over event without experiencing a failure of the canister containment boundary.

This sensitivity study adjusted the baseline model to make it more resilient to the tip-over load case. Steel plate channels were added on the inside of the cask liner to reduce the unrealistic radial gap. Figure 3-14 shows the added channels. This change to the design eliminates the predictions of containment boundary failure, and brings the response closer into the range expected of a certified DSC system.

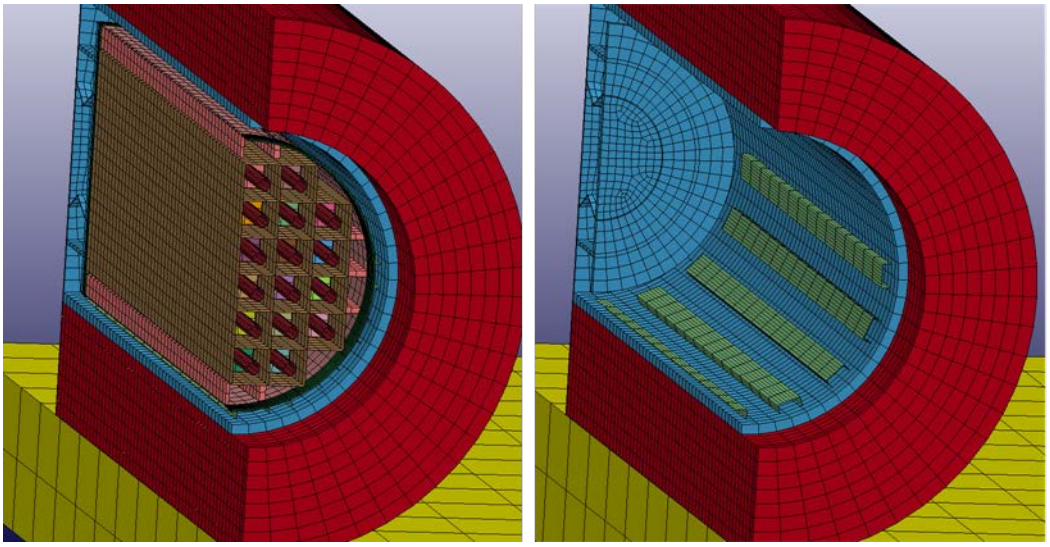

Figure 3-14. Channels Added to Cask

This model was run using double precision as a precaution. The addition of the thin channel plates might have increased the sensitivity of the model to the solver's numerical precision. The presence of the channels reduced the gap size and altered the location of maximum stress and strain in the canister wall. Figure 3-15 shows the plastic strain in the upper canister region at 47 ms. In this case the peak plastic strain occurs in the canister shell at the edge of the cask channel, rather than at the lid weld region, as predicted in the baseline case (compare to Figure 3-4).

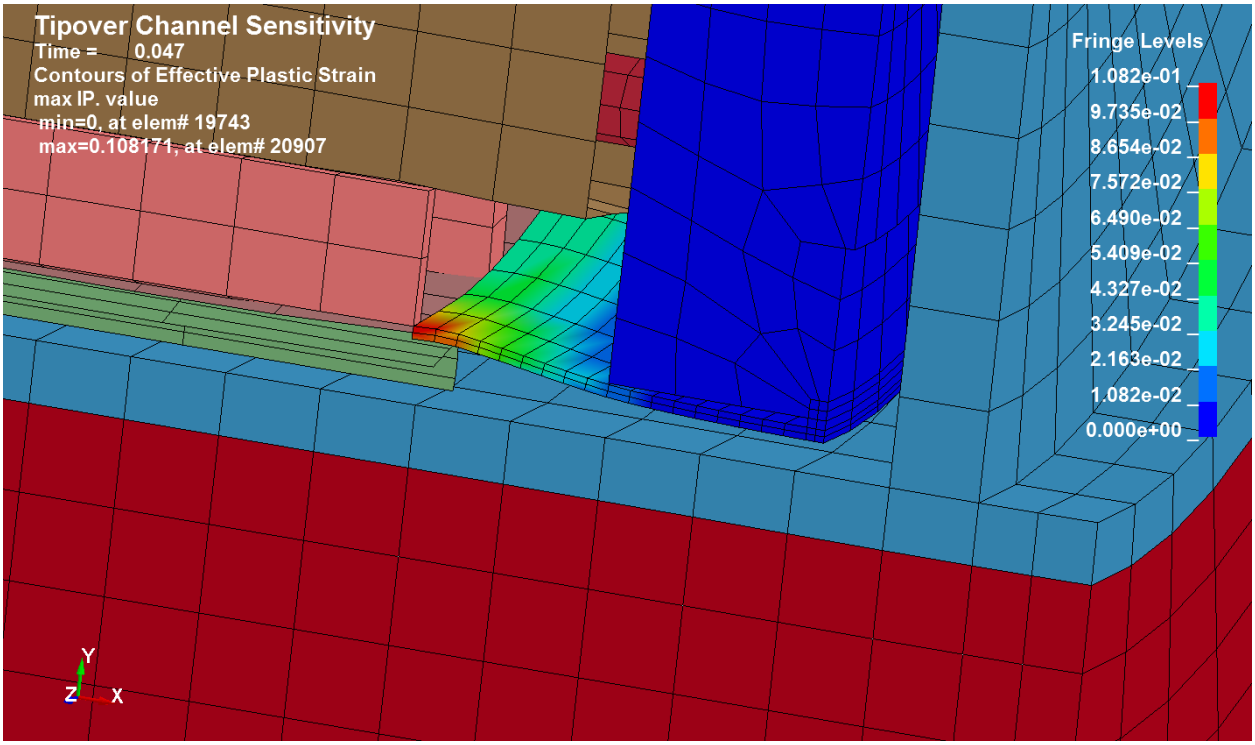

Figure 3-15. Plastic Strain Contours in Lid and Upper Canister Shell

The plastic strain history for a number of elements is plotted in Figure 3-16. H21051 is the element at the top centerline lid weld, the same number plotted in Figure 3-6 and discussed as the peak plastic strain element in Section 3.2. When channels are added, plastic strain is still predicted in the weld region, but it is much less than it was without channels and much less when compared to the new maximums. The other elements plotted in Figure 3-16are identified in Figure 3-17 which shows the highest canister shell plastic strain region. The results show a strong discontinuity between the plastic strains calculated in the shell elements and the solid elements. Because the mesh transition from shells to solids takes place right at the new location of interest, the peak stress and strain values reported by the model are questionable. The general behavior of the model appears reasonable, but a more targeted finite element representation would be needed to determine credible peak stresses and the correct local structural response. It can be concluded that through-wall plastic strains are expected in the shell wall, and some plastic strain in the weld is expected.

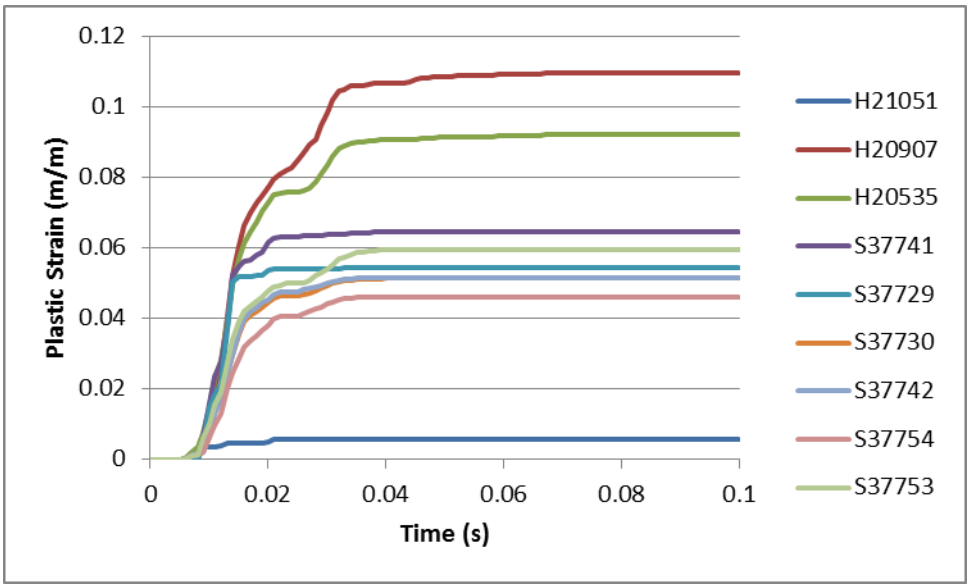

Figure 3-16. Select Element Plastic Strain Histories

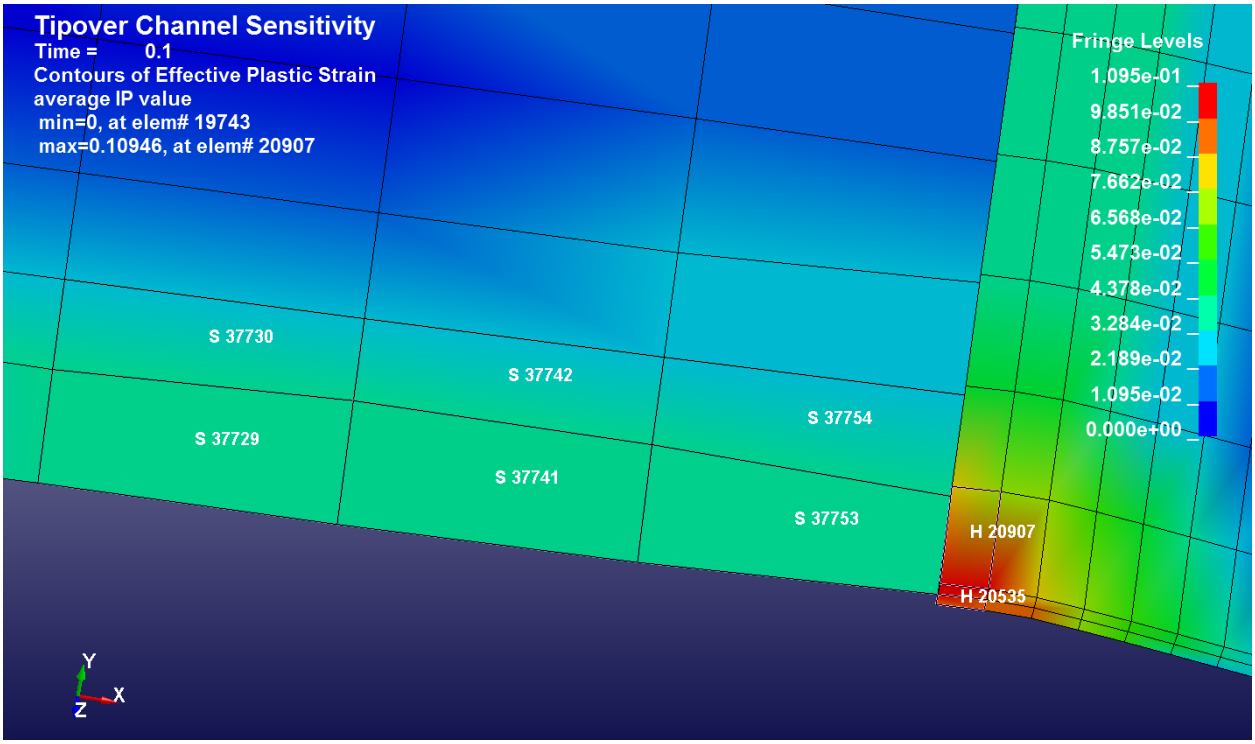

Figure 3-17. Canister Shell Plastic Strain at 100 ms, Select Elements Identified

The baseplate stresses and strains are also affected by the introduction of channels. Figure 3-18 shows the plastic strains with two viewing angles. Most notably, the broad plastic strain region near the impact point is gone (compare to Figure 3-5). Its absence indicates that it was probably attributable to the large radial gap size assumed in the baseline model. There is no longer any through-wall plastic strain in the baseplate, but there is still a localized plastic strain attributed to interaction with the fuel assembly and basket. There are also through-wall plastic strains remaining at the shell to baseplate welds, which are of potential concern for the weld integrity.

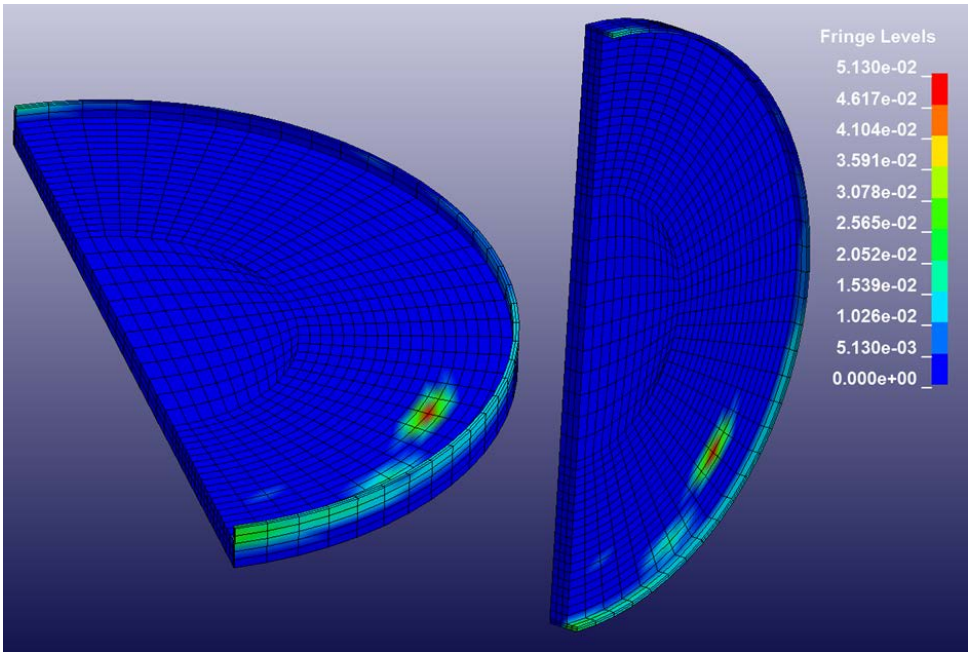

Figure 3-18. Baseplate Plastic Strain with Channels

An interesting effect on the shell wall can be seen in Figure 3-19 when the plastic strains are plotted with a lower range. This model predicted significant areas of the shell wall to have plastic strains, indicating a broad region with stresses above the material's yield strength. Without the channels, there was a broad region of through-wall plastic strain in the baseplate. With channels, a broad region of plastic strain appears in the shell wall. This may be a design-independent consequence of a tip-over scenario.

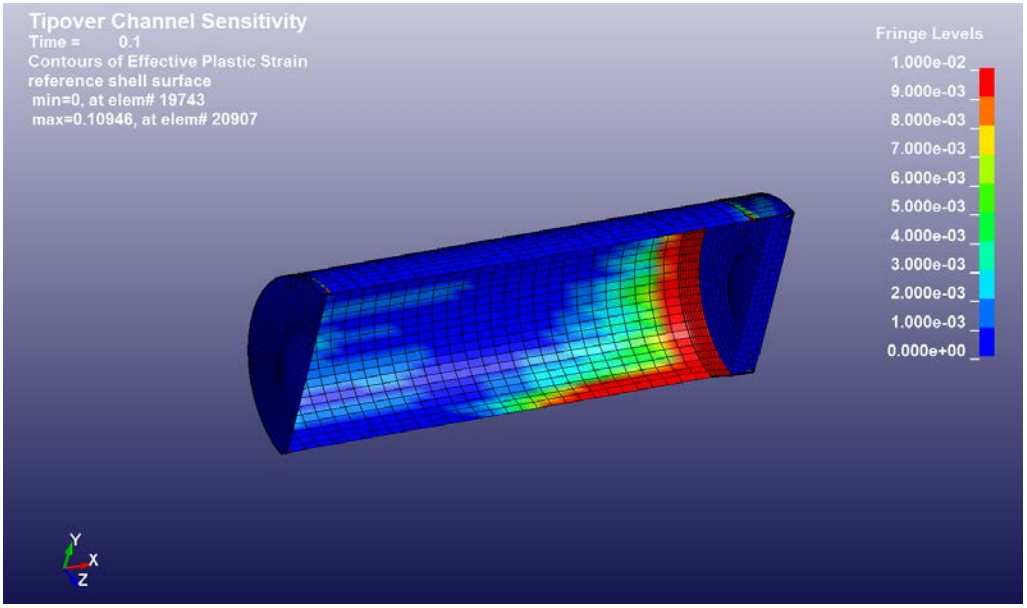

Figure 3-19. Canister Plastic Strains, 0 to 1.0 Percent

The von Mises stresses are summarized in Table 3-2. While the lid weld was no longer above the failure strength, as it is in the baseline case, it did still exceed yield both in peak and through-wall stresses. The canister shell has significant through-wall stress above the yield limit. The base plate to shell weld also exceeded yield. Stresses in many locations around the containment boundary are a concern. Section 3.9 will compare these results to the baseline configuration results and identify areas of common concern.

Table 3-2. Channels Added Tip-Over Stresses

Location	Peak (MPa)	Through-Wall (MPa)
Canister Lid Weld	161	156
Canister Shell Wall Maximum	267	226
(Near Lid Weld)	148	114
(In Shell Elements)	267	226
(In Shell Elements Connected to Basket Rails)	267	226
(In Shell Elements Away from Geometric Discontinuities)	200	176
Base Plate Shell Weld	215	206
Base Plate Through Thickness	146	84

3.6 Sensitivity Study: CSCM Overpack Concrete

The pseudo tensor concrete model has received some criticism in the literature because its damage model is not accurate. The CSCM was implemented as a sensitivity study to determine if a more accurate damage model could affect the results. Preliminary modeling suggested there could be a difference in the calculated dynamic behavior because of the model.

In this sensitivity case the pseudo tensor material of the concrete overpack was replaced with CSCM defined to have an equivalent crush strength. The ISFSI pad was not changed, and remained the baseline pseudo tensor material. This choice was made to keep one of the impacting concrete bodies consistent with the baseline, and the potential damage to the overpack is of more interest to this study.

The results show that the concrete model does not have a significant effect on the maximum strains predicted in the canister. It does reduce the magnitude of the broad plastic strain region in the baseplate, but has little to no effect on the lid weld region.

The biggest difference between the CSCM results and the baseline results is the damage predicted to the overpack concrete. Figure 3-20 shows contours of concrete damage for the CSCM (top) and the PT concrete (bottom), but note that the two material formulations represent damage differently. Even though effective plastic strains are plotted, they mean different things. In the PT case, the plastic strain represents plastic deformation of the material that correlates to softening (reduction in strength) of the material. In the CSCM case, the plastic strain is actually a damage tracking parameter that varies between 0 and 1, with 0 being undamaged and 1 being completely damaged. The fringe level of zero indicates the material maintains its starting strength and stiffness. The fringe level of 1.0 indicates complete loss of strength and stiffness. In the CSCM tip-over case, none of the elements reach a value of 1.0, but widespread damage is predicted within a significant volume of the material. This is interesting because the plastic

strains calculated in the PT case do not suggest such widespread damage. This difference does not have an effect on the containment boundary, but the CSCM offers a different perspective of what can be expected qualitatively to the concrete overpack in a tip-over scenario. The next section considers the effect of a more functional change to the concrete.

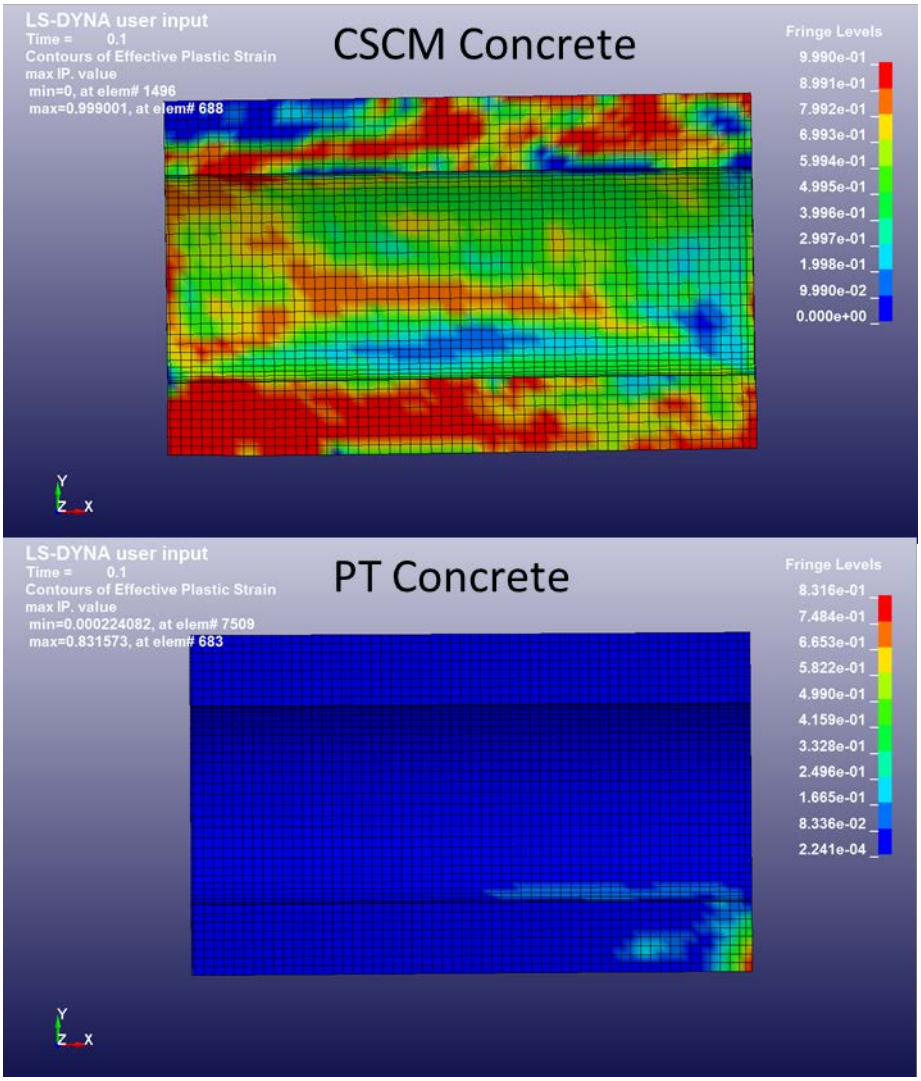

Figure 3-20. Concrete Damage during Tip-over: (top) CSCM. (bottom) Psuedo Tensor Concrete Model

3.7 Sensitivity Study: Concrete Pad Variation

One material feature of the impact scenario that could potentially change over time is the behavior of the concrete ISFSI pad. This sensitivity study was conducted to determine how much of an effect a change in concrete crush strength could have on the tip-over scenario response. Much of the impact energy in the baseline case is dissipated by crushing concrete, so changes to the crush strength were thought to be capable of altering the dynamic and structural response of the DSC system.

The baseline pseudo tensor concrete material model is borrowed from Witte et al. (1998), with the only difference being a change in units. The input parameters of this model were developed experimentally and offer a complex nonlinear behavior that matches the data test data through specific equations of state. LS-DYNA has the capability to automatically generate equations of state for a specified crush strength, and this feature was used in this sensitivity study to generate materials with a plus and minus 20 percent variation off the baseline crush strength. The automatic generation feature was also invoked to generate a material model based on the crush strength, to compare its behavior against the model derived in Witte et al. (1998).

The results of this task show that the baseline tip-over response is not heavily influenced by a +/-20 percent change in concrete crush strength. Even though more total energy is absorbed by the pad concrete, the overpack concrete has potentially more of an effect on the tip-over response because its crushing is more localized and higher in magnitude. Even though it absorbs energy, the pad acts more like an elastic surface than a crushable one.

When both the pad and overpack are replaced with -20 percent crush strength concrete (3360 psi), the containment boundary results were altered somewhat. The peak lid weld material stress dropped to 519 MPa and the through-wall stress dropped to 454 MPa. Compared to the baseline case values of 625 MPa peak/540 MPa through-wall, this suggests the 20 percent reduction in both cask and pad concrete crush strength resulted in a 15 to 20 percent reduction in stress in the critical containment boundary location.

This study concludes that concrete crush strength has a potential effect on the containment boundary stresses that could potentially be proportional to the change in crush strength of the overpack concrete. Changes to the ISFSI pad material showed no significant change in the results of interest, but one factor that was not explored was the sensitivity of changing crush strength to the ISFSI pad mesh density. The tip-over impact contact occurs along two rows of elements in the overpack, but only one row of elements in the pad. For this reason, it is recommended that the ISFSI pad material not be ruled out for future study in an extended dry storage setting, but it would be reasonable to treat the cask material with a higher priority.

3.8 Sensitivity Study: Long Duration

The baseline case was run out to two seconds of model time. This duration is sufficient to dissipate the kinetic energy of the tipped DSC system down to 0.005 percent of its starting value. For comparison, at 100 ms the DSC system kinetic energy is down to 9 percent of its starting value, with a rebound velocity vector that is pointed upwards and horizontal. After 100 ms, the cask system has to fall back to the ISFSI pad and remain in contact long enough for friction to halt its horizontal progress.

The rigid body motion of the DSC center of mass is plotted in Figure 3-21. The positive peaks represent impacts, or net decelerations of the system. Accelerations below zero indicate freefall, when the system is being pulled down by gravity. Almost all of the permanent structural deformations of interest occur within the 40 ms of peak **a**. The 40 ms encompasses the primary impact of the canister lid end and the subsequent primary impact of the base plate end. Additional plastic deformations in the elements of interest occur up to 100 ms, with slight increases possible out to 500 ms. To put it in perspective, the plastic strain in the lid weld

element #H21051 was recorded as 16.4 percent at 100ms, and increased to 16.5 percent at 450 ms, where it remained through 2 seconds (or 2000 ms). While the plastic strain does increase after 100 ms, it is not worth the computational cost for this study to run every case to this extreme duration.

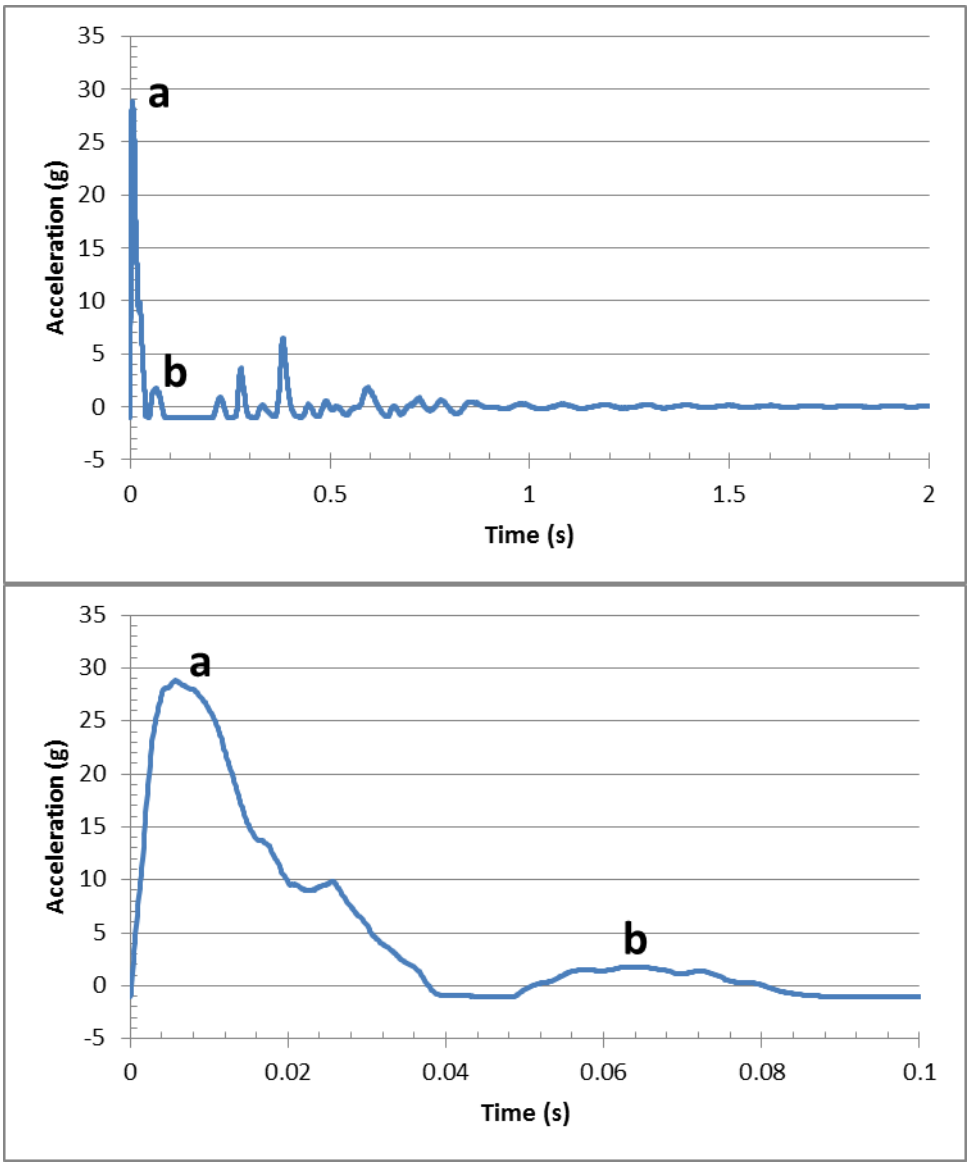

Figure 3-21. DSC Rigid Body Acceleration, a) is the major impact, b) is a secondary impact. Impacts after b) do not cause additional plastic deformation.

3.9 Tip-over Case Summary

In total, eight tip-over analyses were performed to explore the response of a generic DSC system. Cases like the double-precision (Section 3.2) and extended duration (Section 3.8) demonstrated that the fundamentals of the analysis are sound, that the single-precision solver and the 100 ms duration are adequate for this study. The CSCM concrete case was interesting for its prediction of concrete overpack damage (Section 3.6) but it did not affect the containment boundary

response, which was the focus of this study. The concrete pad variation (Section 3.7) results suggested that concrete degradation or hardening are of secondary interest.

The multilinear material case (Section 3.4) demonstrated that changes to the stress-strain curve in the plastic strain region can alter the calculated stress and strain values, but for the baseline geometry the same conclusions are reached: through-wall plastic strains are predicted at locations in the containment boundary, and through-wall failure of the lid weld region is predicted for the baseline design. The results of this case led to the conclusion that the geometry of the baseline system is to blame for the high stresses calculated through the lid weld region. While some existing canister designs have similar geometry, the stresses they develop during tip-over cannot be as high as predicted in this study.

While its stresses are considered to be unrealistically high, the baseline model (Section 3.1) provides quantifiable stress results for all the regions of the canister containment boundary. The increased mesh density case (Section 3.3) is used to define the key stress values (Table 3-1) because the higher mesh density is expected to calculate more accurate results. The baseline geometry allows the canister edge to directly impact the cask liner, which puts tremendous deformation energy into the lid weld region.

The channel-added geometry (Section 3.5) modifies the baseline design to reduce the initial gap size and introduce steel plate channels to better distribute the impact energy. The stresses for this case were based on the baseline model mesh density and were summarized in Table 3-2. The channels move the critical high stress region from the lid weld (in the baseline case) to the canister shell wall, where the top of the channels terminate. While stresses in this case were predicted to be much lower than the baseline case, it still predicts significantly high through-wall plastic strains.

The strain rates in both cases are high, but the baseline geometry has strain rates that are an order of magnitude higher (151 vs. 16 m/m/s). These rapid strains happen in the weld material in the baseline case and in the canister shell in the channel case. Both cases could involve weld material, if the channel case impact line happens to align with a longitudinal shell weld.

In the baseline case, the lid weld exceeded its ultimate strength, which can be considered a failure of the containment boundary. The radial gap size assumed in these calculations has a strong contribution to this excessive stress state, as well as the thickness of the canister wall. Vendor specific designs have been analyzed for tip-over and have been licensed by the NRC because they do not result in this potential failure. But the conclusion from a materials standpoint is that material behavior of welded joints at high strain rates is critical topic of interest for long term storage analyses. It is not only the lid weld in the baseline case, but also the base plate weld and the longitudinal cask shell welds that experience high stresses and plastic strains. Possible imperfections in the welds are an important consideration, as well as any processes that can potentially degrade the quality of welds over time.

Future work is planned to quantify how much degradation would be necessary for failure of the containment boundary to occur and will also focus on the fuel assembly and cladding behavior under these conditions. One recommendation for future work is to accurately model existing DSC systems to determine realistic tip-over design margins.

4. HANDLING DROP LOAD CASE

Like the tip-over case, initial models for the handling drop case were focused on determining general response behavior and mesh density needs. It was concluded that the same model used for tip-over would be adequate for the handling drop. The gravity load was applied on the initial time step, rather than performing an additional preload step. No significant response effects were noticed in the calculated results.

The primary load was an initial downward velocity of 2.4 m/s, which corresponded to a drop height of 12 inches (0.3m). The canister made contact with the cask base weldment structure, which translated the load down to the concrete ISFSI pad. The concrete absorbed most of the impact energy through crushing. By 0.1 seconds, most of the kinetic energy was dissipated and the system had reached a state of rest.

In general, the loads caused by the handling drop were much lower than the tip-over case and did not present any challenge to the containment boundary. Section 4.1 discusses the baseline model results using the pseudo tensor concrete material. Section 4.2 discusses the use of CSCM. Section 4.3 discusses a sensitivity case with an increased strength assigned to the concrete. Section 4.4 summarizes the handling drop evaluation.

4.1 Baseline Handling Drop

The handling drop proved to be a much less potentially damaging case than tip-over. The lid weld region experienced a peak instantaneous stress of about 80 MPa, which was much lower than the assumed yield limit of 148 MPa. The canister shell experienced a peak element stress of about 126 MPa, with peak nodal stresses reaching 148 MPa. These peak values may have been artificially high because they occured at a stress concentration on the solid element involved in the shell-to-solid transition near the base plate. On the shell side the peak was only 106 MPa, and again this may have been affected by the shell-to-solid element transition. Away from the transition, the peak stress in the canister shell was about 80 MPa.

At the shell-to-baseplate weld, the peak stress reached 148 MPa, which was the yield strength threshold. The baseplate had an interesting plastic strain response that was influenced by the geometry of the liner base weldment. Figure 4-1 shows the plastic strain contours in the canister, and Figure 4-2 adds the surrounding cask (overpack) liner and base weldment structure. The cylinder of the weldment was relatively rigid and localized the load on the canister base plate. Variations in weldment design might have a different effect on the baseplate, but the one modeled is considered to be reasonably representative. Any realistic weldment design can be expected to offer nonuniform reaction forces. In this case, the peak plastic strain was less than 1 percent. The peak baseplate stress reached 149 MPa, and the maximum average through thickness stress was about 113 MPa (both von Mises). In terms of maximum shear stress, the peak was 84.8 MPa and the maximum through-wall average over time was 64.7 MPa.

The von Mises stresses are summarized in Table 4-1.

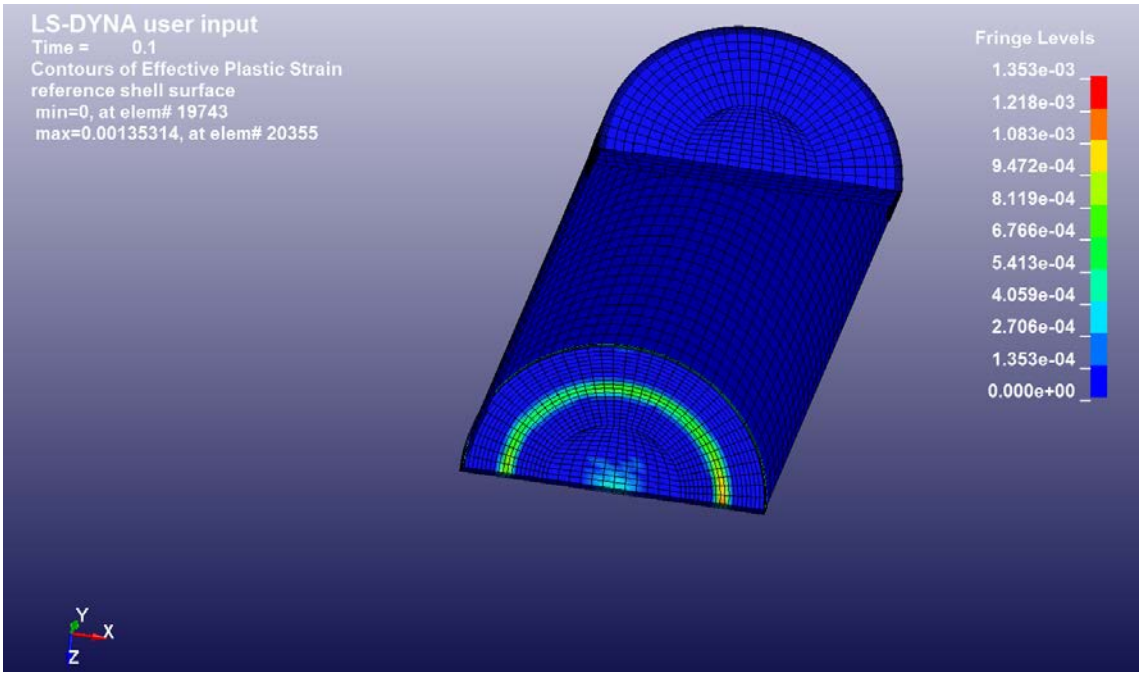

Figure 4-1. Handling Drop Plastic Strain

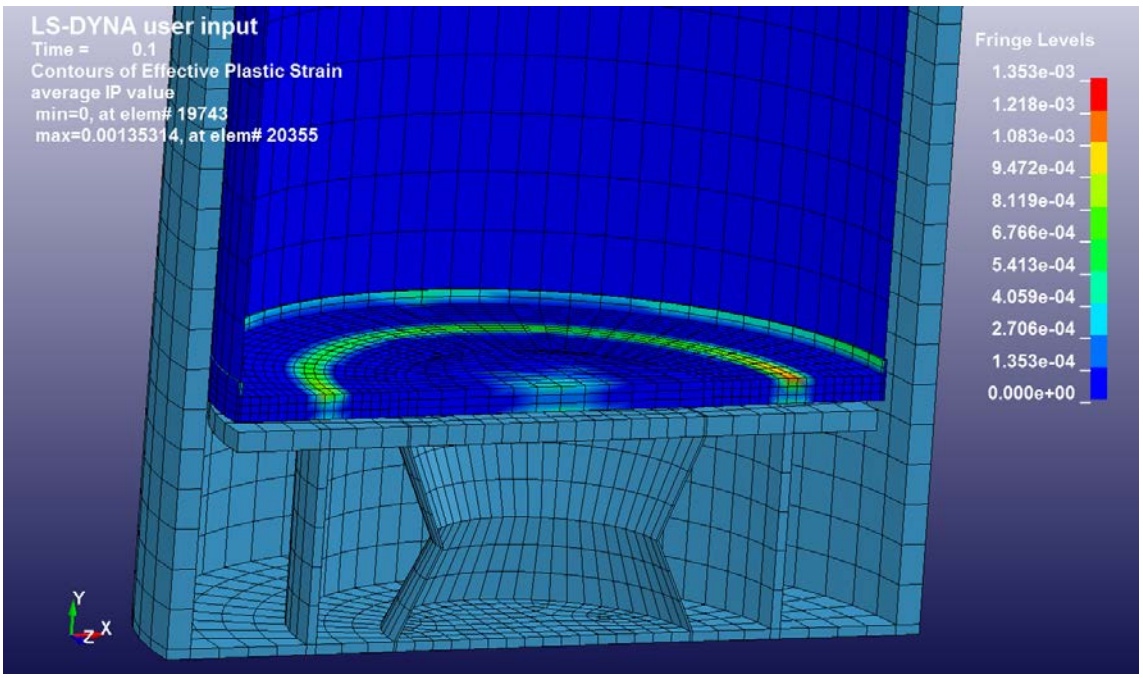

Figure 4-2. Canister Plastic Strains in Canister with Cask Liner and Base Weldment

Table 4-1. Baseline Handling Drop Stresses

Location	Peak (MPa)	Through-Wall (MPa)
Canister Lid Weld	78	74
Canister Shell Wall Maximum	106	98
(Near Lid Weld)	53	36
(In Shell Elements)	106	98
(In Shell Elements Connected to Basket Rails)	106	98
(In Shell Elements Away from Geometric Discontinuities)	56	55
Base Plate Shell Weld	148	90
Base Plate Through Thickness	149	113

The maximum fuel assembly acceleration response occurred in one of the two most central fuel assemblies. The peak deceleration was 60.5 g, as plotted in Figure 4-3. . This is a different loading situation on the fuel than the tip-over case because the forces went through the lower tie plate of the fuel assembly, rather than the horizontal orientation loading of the tip-over.

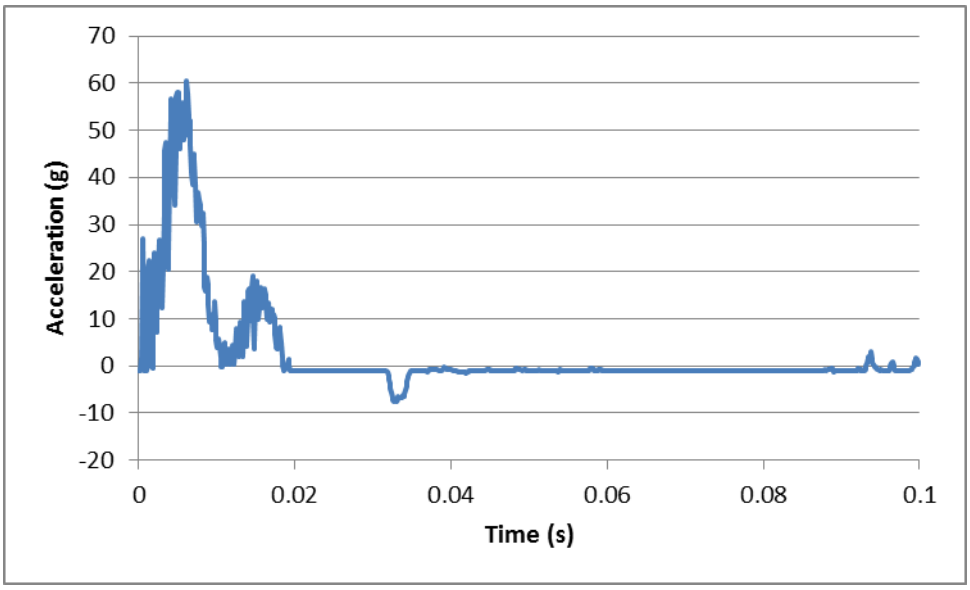

Figure 4-3. Fuel Assembly Drop Response

4.2 CSCM Concrete Sensitivity Study

The CSCM concrete case results are essentially identical in regards to the response of the canister containment boundary. Peak stress in baseplate/shell weld region is 148 MPa. Peak von Mises stress in the base plate at the stress concentration caused by the weldment is 149 MPa, with a maximum through-wall von Mises stress of 115 MPa. At the same location the maximum shear stress is 84.9 MPa peak and 66.2 MPa through-wall.

As in the tip-over case, the primary difference is the damage prediction capability of the CSCM. Figure 4-4 plots the CSCM damage parameter (left) and the pseudo tensor plastic strain (right). In this case CSCSM model predicts more significant damage to the concrete near the bottom, but otherwise the damage patterns are similar. It can be concluded that the CSCM concrete does not have any significant effect on the handling drop response.

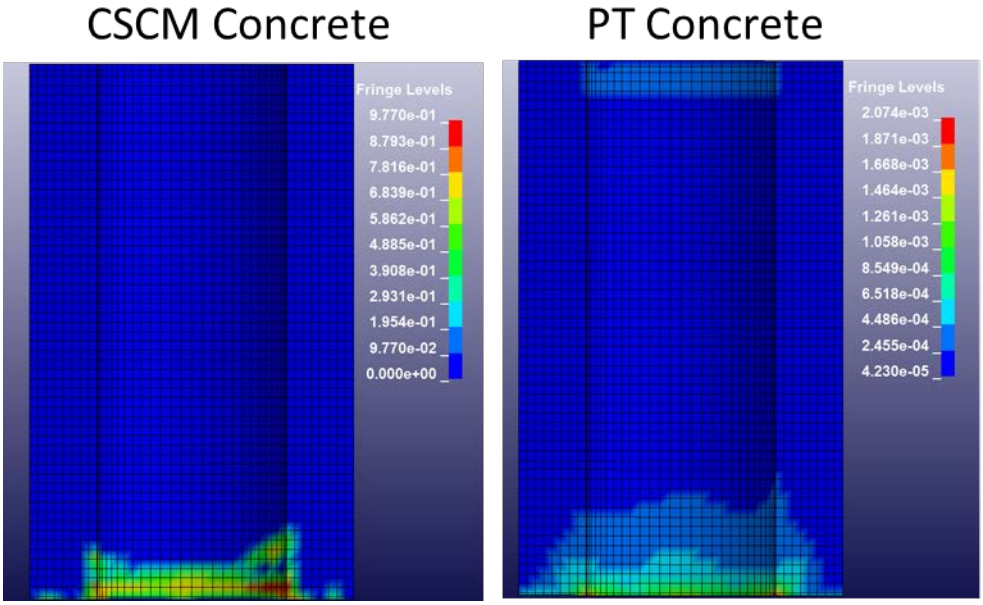

Figure 4-4. Concrete Damage in CSCM Concrete (left) and Psuedo Tensor Concrete (right)

4.3 Concrete Strength Sensitivity Study

The concrete pad compressive strength was increased by 20 percent using the concrete pad variation discussed in 3.7. In the tip-over case, the changes in ISFSI pad crush strength did not lead to any significant change in structural response. In this handling drop case, the 20 percent increase in concrete crush strength has a minor effect on the stresses of the containment boundary. Changes in stress are all less than 10 percent. It does have a nearly proportional effect on the fuel assembly peak acceleration, which increases to about 71 g. The stresses are presented in Table 4-2. The maximum stress location is in the base plate above the weldment cylinder, with von Mises stresses of 146 MPa peak and 119 MPa through-wall. In terms of maximum shear stress, the peak and through-wall stresses were 84 MPa and 68 MPa, respectively.

Table 4-2. Handling Drop +20 Percent Crush Strength

Location	Peak (MPa)	Through-Wall (MPa)
Canister Lid Weld	87	82
Canister Shell Wall Maximum	113	104
(Near Lid Weld)	59	41
(In Shell Elements)	113	104
(In Shell Elements Connected to Basket Rails)	109	104
(In Shell Elements Away from Geometric Discontinuities)	97	67
Base Plate Shell Weld	131	91
Base Plate Through Thickness	146	119

4.4 Summary of Handling Drop

The handling drop case represents a drop of the canister into the cask with a free-fall distance of 12 inches. Peak stresses occur in the canister base plate, above the base weldment cylinder. Surface stresses reach 149 MPa, which is slightly above the yield strength of 148 MPa. Through wall stress reaches 113 MPa, which indicates most of the thickness remains elastic. This stress state is not expected to be a failure concern for the material in pristine condition.

Additional high stresses of potential interest occur at the base plate to canister shell weld, where the peak and through-wall stresses reach 148 MPa and 90 MPa, respectively. This is a lower stress state than the base plate, but this location has the added complexity of a weld. The weld can potentially add a stress concentration factor that was not considered in the model. This is potentially the weakest location of the containment boundary because it involves a weld.

From an extended storage standpoint, the handling drop is of most concern at the end of an extended period of dry storage. This load case might potentially happen when a canister needs to be transported, or transferred from one vertical dry storage cask to another. Any processes that can lower the yield strength or lower the ductility are a concern for the containment boundary. Also, any process that can gouge the material or erode the cross-sectional thickness can potentially raise the local stresses. Future work is planned to quantify how much degradation would be necessary for failure of the containment boundary to occur and will also focus on the fuel assembly and cladding behavior under these conditions.

The baseplate weld looks like the most vulnerable location on the containment boundary because of its high stresses and the potential variability of the weld quality. Any process that can degrade the quality of the weld over time would be an important containment concern, as well as any process that could effectively cause a stress concentration in the weld region.

In this handling drop case the lid weld is not a primary concern because its stresses are significantly lower than the base weld. Stresses would have to nearly double before the lid weld became a containment concern. Because of the importance of the lid weld it is not expected that it would be of low quality, but if welds are susceptible to degradation over time by some natural process it is worth considering its effect on the lid weld.

The variation in concrete strength does not have a strong influence on the calculated stresses. The peak fuel assembly acceleration increased proportionally with pad crush strength, but stresses remain approximately the same.

5. SEISMIC EVALUATION

Initial modeling explored a fully three dimensional (3D) load case with a highly disfeatured model of the DSC system. It was determined that a full 3D load case using the baseline model geometry as a basis would not be feasible because of the computational requirements. It was also determined that a model that was defeatured enough to run with a 3D seismic load would not have enough detail remaining to provide valuable results. Instead, the half symmetry baseline model would be used with one vertical and one horizontal acceleration history load.

5.1 Seismic Load Construction

The goal of the seismic load case was to apply a ground excitation to the pad that was similar to the earthquake that affected the North Anna power station on August 23, 2011. Time history data describing the earthquake is publicly available from the U.S. Geological Survey (USGS) and other earthquake monitoring networks from monitoring stations as near as 53 km away. The magnitudes of peak acceleration and velocity at that distance were lower than what was reported at the North Anna site, so the loads were scaled up to approximate the earthquake intensity. This construction process was expected to lead to a reasonable approximation of the earthquake at North Anna, without precisely matching it.

The specific time history set used was from the Charlottesville monitoring station, which was 53.5 km from the epicenter, and witnessed a peak horizontal ground motion of 0.121 g. The raw data was downloaded from the Center for Engineering Strong Motion Data (CESD) web site, which provides access to data from a number of earthquake monitoring stations (CESD 2013).Based on USGS shakemap data (USGS 2009), the expected range of ground motion for the North Anna site could have been up to the Very Strong category, with peak accelerations between 0.18-0.34 g and peak ground velocity between 16-31 cm/s. Of the two available horizontal directions, denoted as 90 Degrees and 360 Degrees, the 360 Degree record was selected to represent the horizontal motion of half-symmetry model because it has the strongest peak of the two.

The raw data were filtered with a high-pass Butterworth filter with a cutoff frequency of 0.125 Hz to eliminate the low frequency content of the raw data. This removed the natural drift that occurs when acceleration signals are integrated over relatively long durations and kept the velocity and displacement centered about zero. When the filtered acceleration data were integrated to determine velocity and displacement, they compared well to the baselined data provided by the USGS. The removal of the low frequency content by the filtering operation did alter the character of the recorded acceleration history, but because the effect on the peak acceleration (<1 percent) and velocity (<10 percent) were small, it was concluded that the low frequency content can be reasonably removed without leading to a significant alteration of the earthquake's character.

After filtering, the acceleration and velocity magnitudes did not meet the levels predicted for the North Anna site, reaching peaks of just 0.12 g and 1.5 cm/s, respectively. From the USGS data, it was apparent that the ground motion experienced at Charlottesville was much lower than at North Anna, so some adjustments were made. The first adjustment was to amplify the Charlottesville data by a factor of 2.8, which brought the peak acceleration to 0.34 g (the upper

limit of the Very Strong category) and the peak velocity to 4.1 cm/s (which is still below the minimum velocity of the Very Strong category.) This was evaluated as Seismic Load Case #1.

While Load Case #1 matched peak acceleration, the fact that it fell short of the expected velocity range indicated the rigid body motions caused by this case are not representative of the North Anna scenario. One notable observation from North Anna was that some of the dry storage casks on the ISFSI were moved out of position by the earthquake, up to about 4.5 inches (11 cm), as reported by Grecheck (2011). In contrast, the ground motion displacement derived by double integrating the Load Case #1 only reached a maximum displacement of 0.87 cm. Preliminary results of the DSC response to this load case demonstrated very little relative motion between the base mat and the cask system.

In order to achieve more representative rigid body motion of the pad and cask system, Load Case #2 was constructed using an amplification factor of 12.8. This causes the peak instantaneous acceleration to reach 1.56 g, well above the value expected at North Anna, but caused the peak velocity to reach 18.8 cm/s, which fells within the Very Strong range of 16-31 cm/s. While the instantaneous acceleration in this case was higher than desired, the focus of this second seismic load case was the rigid body response of the system. A brief acceleration spike was not expected to cause a significant rigid body response from the DSC system or lead to a significant artificial structural response. As the next section will discuss, the fundamental difference between the Charlottesville data and the North Anna data is in the frequency domain, which is not something a simple scaling operation like the one used here can address.

The best way to analyze the DSC system response to the North Anna earthquake would be using the acceleration data recorded on site, with the specific dry storage cask systems modeled. The two load cases studied here represent something of similar magnitude and response. The modeling was sufficient for its purpose, to identify trends in the structural response, but cannot be considered to be predictive of what happened to the DSC systems at North Anna.

5.2 Seismic Load Case Response Spectra

The two load case acceleration histories were analyzed using one degree of freedom systems to calculate their frequency response spectrum. Five percent damping was assumed. Responses were calculated for whole-numbered frequencies between 1 and 99 Hz and are plotted in Figure 5-1. The horizontal and vertical cases refer to Load Case #1, while the maximum horizontal and vertical cases refer to Load Case #2. This response spectrum can be used to compare the seismic load cases used in this study with other earthquakes. One thing to note is that even though the peak instantaneous accelerations are similar, the vertical load invokes a significantly higher response than the horizontal load across the whole frequency band. Another thing to note is that the peak frequencies are between 10 and 20 Hz, and the response is at its minimum at 1 Hz. Comparing this frequency response plot to the ones reported for the North Anna power station by Grecheck (2011), the maximum vertical case envelopes North Anna, but the maximum horizontal does not envelope it below 10 Hz. This probably explains why the amount of lateral cask motion predicted by the model for Load Case #2 is still short of the values experienced at North Anna, which will be discussed more in Section 5.4.

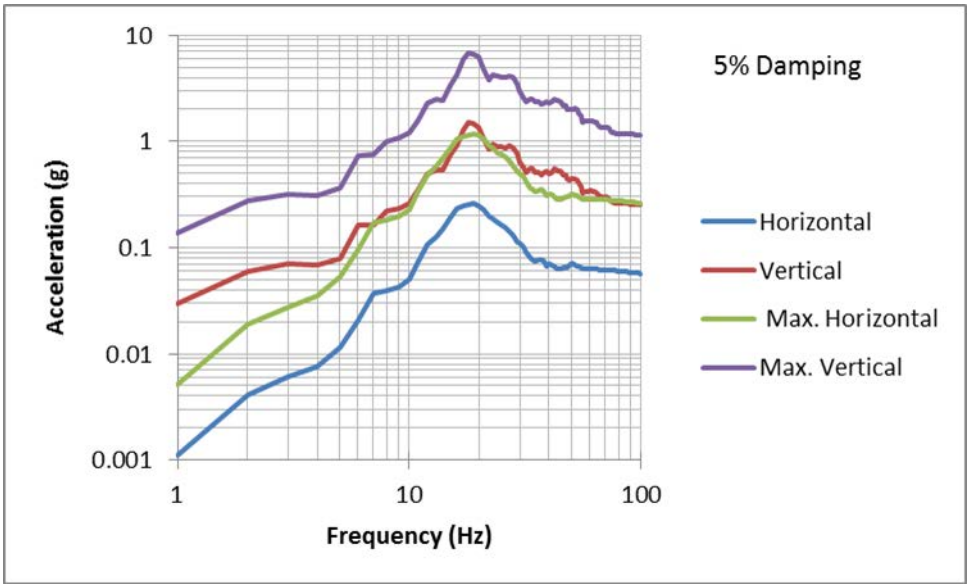

Figure 5-1. Frequency Response Spectra of Seismic Load Cases

5.3 Results of Load Case #1

The response to Seismic Load Case #1 was very mild in terms of stresses and strains. The final horizontal displacement of the DSC system relative to the concrete pad was less than 0.5mm. This is consistent with the peak horizontal displacement of the pad, which only reached about 6mm. Vertically, the DSC system raised upward a maximum of about 4mm and dropped a maximum of 7mm before returning to its starting elevation. The DSC System center of gravity responded with a maximum horizontal acceleration of 0.4 g and a vertical acceleration of 1.3 g. The peak fuel assembly acceleration reached 1.9 g. The maximum stresses are listed in Table 5-1. By all measures, this was a mild earthquake load that caused a mild stress response in the containment boundary. Even though this case was inspired by the earthquake that affected North Anna and the peak acceleration is in the expected range, the peak velocity and the lower frequency components of the load case are below what is expected to have occurred at the North Anna site. Load Case #2 increases the magnitude of the ground motion, as discussed in the next section.

Table 5-1. Seismic Load Case #1 Stresses

Location	Peak (MPa)	Through-Wall (MPa)
Canister Lid Weld	4	4
Canister Shell Wall Maximum	39	28
(Near Lid Weld)	2	2
(In Shell Elements)	39	28
(In Shell Elements Connected to Basket Rails)	39	28
(In Shell Elements Away from Geometric Discontinuities)	24	17
Base Plate Shell Weld	20	14
Base Plate Through Thickness	22	14

5.4 Results of Load Case #2

Seismic Load Case #2 was amplified substantially in both the vertical and horizontal directions. As discussed previously, the Charlottesville data were amplified by a factor 12.8 to put the peak velocity in the range expected to have occurred at the North Anna site. However, from the frequency response analysis in Section 5.2, the major difference between the Charlottesville and North Anna data looks to be in the frequency domain, rather than a straight scaling of the amplitude. This load case appears to envelop the North Anna response in the vertical direction, meaning that the model results are expected to bound the values that would be expected of a more precise representation of the North Anna vertical load. In the horizontal direction, though, Load Case #2 does not envelop the North Anna response in the frequency range below 10 Hz. The vertical loads are expected to be the primary drivers of stress and strain, while the horizontal loads could potentially alter the contact points between the canister and the cask liner or base weldment.

In the horizontal direction, the DSC experiences a relative change of position on the pad of 15 mm by the end of the analysis. The maximum movement recorded at the site was 4.5 inches (110 mm), but the minimum movement was zero. This suggests that Load Case #2 may be sufficiently bounding in its stress calculations to represent at least some of the North Anna casks, but it does not provide all the insight a detailed study of the North Anna cask behavior might reveal.

The peak stress response is reported in Table 5-2. The peak stress occurs in the baseplate, right above the weldment cylinder. This is the same location as the peak in the handling drop case, though its magnitude is significantly lower, with a peak stress of 49 MPa and a through-wall stress of 32 MPa. These stresses are very low, compared to the yield strength of 148 MPa.

Table 5-2. Seismic Load Case #2 Stresses

Location	Peak (MPa)	Through-Wall (MPa)
Canister Lid Weld	17	16
Canister Shell Wall Maximum	45	30
(Near Lid Weld)	9	8
(In Shell Elements)	45	30
(In Shell Elements Connected to Basket Rails)	45	30
(In Shell Elements Away from Geometric Discontinuities)	45	29
Base Plate Shell Weld	47	33
Base Plate Through Thickness	49	32

In this seismic case, a fatigue assessment might be of interest. Over the 40 second duration of the analysis, the frequency content of the peak stress element was analyzed and found to have a primary peak near 10 Hz. If we assume the peak stress of 49 MPa occurs at a cyclic rate of 10 Hz for a duration of 40 seconds, this adds up to just 400 cycles. For extended storage considerations, it might be prudent to assume a similar earthquake happening every 100 years or every 10 years. If we assume the same earthquake happens every 10 years for 300 years, the

number of cycles only reaches about 10^4 cycles. Fatigue strength tends to fall off more in the range of 10^5 cycles, and there does not seem to be any reasonable way to reach that value.

5.5 Summary of Seismic Results

The seismic load cases apply vertical and horizontal acceleration histories to a section of ISFSI pad to investigate the response of DSC system supported by the pad. The acceleration histories are scaled-up versions of the earthquake recorded on August 23, 2011 by the USGS at the Charlottesville, Virginia monitoring station. Ultimately, both of the seismic load cases in this study have similarities to, but are distinct from, the earthquake that affected the North Anna power station, which is about 53 kilometers from North Anna. The load cases are used to predict the type of loads and stresses that can be expected from an earthquake similar to North Anna, but a more precise modeling effort would be needed to calculate the actual response of North Anna's vertical DSC systems.

The stresses on the canister containment boundary are relatively low throughout the structure. Load Case #2 is used as the results of record because they are higher than Load Case #1 and the load case appears to envelope the vertical response of North Anna. The peak stress of 49 MPa occurs in the canister base plate, above the cask base weldment cylinder. This is about one third of the material yield strength of 148 MPa. A significant amount of stress increase would be needed to challenge the containment boundary. When the transient stress history is considered for fatigue evaluation, the number of credible cycles during extended storage is well below the range of concern.

In terms of materials research for long term storage, the issues of concern would be any phenomena that could drastically decrease the cross sectional thickness or the yield strength. Another consideration is any process that could put a stress concentration factor on the surface of the structure, like a gouge in the surface or a localized defect. Weld quality factors might also have an influence on the base plate to shell weld, which is nearly as highly stressed as the base plate. The base plate weld looks like the most critical location on the containment boundary because of the weld. The base plate has higher stresses, but the base plate is composed of one solid piece of material. Any imperfections in the base plate weld would cause a stress riser that was not accounted for in the model.

Future modeling work will focus on determining how much the thickness of sections can be decreased by degradation before the containment boundary becomes challenged, and how large of a crack in the container or weld would be needed to fail the containment boundary at the stresses predicted in this study.

6. CONCLUSIONS

This study analyzed a vertical DSC in three loading scenarios: tip-over, handling drop, and seismic response. The DSC canister containment boundary was most sensitive to the tip-over load case. Depending on the design assumptions, the lid weld or a region of the canister shell experienced localized stresses and plastic strains that could potentially indicate material failure and a breach of the containment boundary. It must be emphasized that this predicted containment failure is an artifact of the generic system modeled. Vendor specific designs analyze for cask tip-over and these analyses are reviewed and approved by the NRC and do not result in failure. The tip-over case that included channels inside the cask had substantially lower peak stresses than the case without, but through-wall plastic straining was still predicted.

A second location of concern for both tip-over configurations was the base plate weld. In both configurations the weld region experienced through-wall plastic strains. The quality of the weld could potentially affect the stress state, but this was not modeled.

After the tip-over case, the canister containment boundary was most sensitive to the handling drop. The baseplate reached localized stresses above the yield limit, but through-wall stress remained below yield. Stresses in the base plate weld were somewhat lower, but they are potentially more concerning because they occur in welded material. An imperfect weld could introduce a localized stress concentration that leads to increased stresses. Since the base plate is a solid section of material, there is no similar geometric imperfection that would increase stresses beyond those calculated in the model.

The seismic load case caused the least amount of concern for any location on the canister containment boundary. Calculated stresses are all below the yield strength of the material. Even considering the seismic response as a cyclic fatigue load, there is no credible challenge to the containment boundary. The only caveat is that because of the random nature of earthquake loads, there will always be some uncertainty about the exact dynamic response of the system. This study selected one set of recorded earthquake motion and applied it to a deterministic model with two scaling factors. This does not bound the loads that could be expected at every ISFSI in the United States, but it does suggest that an earthquake would need to be of high magnitude and duration to challenge the canister containment boundary.

Beyond the containment boundary, the models in this study also predicted the dynamic behavior of the fuel assemblies within the canister. In the tip-over case, it was noted that the peak fuel assembly reached a peak vertical acceleration of 161 g and a peak axial acceleration of 40 g, with indications that the fuel assembly interaction with the base plate could be strong enough to cause plastic deformation in the base plate surface. In the handling drop case, the fuel assembly reached 60 g, and is proportionally sensitive to variations in concrete pad crush strength. The defeatured models used in this study are not accurate enough to precisely define the fuel assembly response, but the magnitude of these loads suggests the fuel assembly structural response should be evaluated to determine the retrievability of the fuel assemblies in these load cases, particularly in the tip-over case.

Section 6.1 discusses the key failure margins and the type of load increases that are needed to cause a failure of the containment boundary. In this context, failure margins refer to the

calculated stresses or strains and the amount of increase it would take to fail the containment boundary. Section 6.2 recommends specific material testing and additional modeling based on the results of this study.

6.1 Key Failure Margins

The most critical canister location and load case of this study is the lid weld in the baseline tip-over scenario. The model predicts through-wall stresses of 594 MPa in the high mesh density case, and this indicates material failure all through the cross section. One physical phenomenon that might alter this prediction of containment boundary failure is to take into account the strain rate behavior of stainless steel. With predicted strain rates reaching 150 m/m/s, this is well outside the commonly available set of material data. If this kind of strain rate data was available, it could be implemented in the model to make a better assessment of the likelihood of failure.

The assumed radial gap of 3 inches (76 mm) between the canister and the cask liner in the baseline case may be excessive compared to existing designs, but gaps of a non-negligible size are expected. If this gap were reduced, a lesser impact with lower impact energy would be expected. The peak through-wall stress was calculated to be 594 MPa, whereas the yield strength is 148 MPa and the ultimate strength is 483 MPa. Using the calculated stresses as an estimate, the load would have to be reduced by about 20 percent to lower the stress below the ultimate strength limit, and by more than 75 percent to lower the stress below the through-wall yield limit. These are just estimates, and ignore the fact that these stresses are all in the plastic strain range, but it seems unlikely that changes to the gap will completely reduce the lid weld stresses to the point that they are no longer a concern for the containment boundary. In the case with channels and a lower effective gap, the lid weld region still experienced through-wall stresses of 156 MPa. It has to be assumed that without the presence of the channels the stress would be higher. Based on these observations, the high stress through the lid weld is considered a general concern for the containment boundary in tip-over, not simply an artifact of the geometry choices. More detailed modeling of actual system designs might arrive at different failure margins, but it is expected that the high strain rate behavior of stainless steel would still be identified as a critical unknown.

In the design with channels, the critical stress location during tip-over shifted to the canister shell wall, near the impact point with the top of the channel. The stress results show a broad region of plastic deformation of the canister shell along its contact path with the channel, so the concern for the containment boundary is not completely localized. The peak through-wall stress is 226 MPa, or 50 percent higher than yield strength. This stress would have to more than double to reach through-wall ultimate strength limit, but because this is well into the nonlinear plastic strain range the actual margin is hard to estimate. Stresses through the shell could potentially increase if impact occurred along a longitudinal shell weld. This is another case where the high strain rate behavior of stainless steel weld material would be useful. Strain rates reached 16 m/m/s, an order of magnitude lower than in the baseline case, but still high compared to the available data. Physical processes that could potentially increase the stresses above what was calculated include surface corrosion, pre-existing surface defects, cracks, or weld imperfections. Accounting for high strain rate behavior might increase the failure margin by raising the effective yield or failure strength.

The circumferential base plate to shell wall weld reaches high peak and through-wall stresses in the tip-over and handling drop cases. The tip-over cases reach through-wall stresses of 210 MPa, with negligible difference between the cases. The plastic strain rate peaks about 8 m/m/s in the tip-over case, which is less than the other strain rates of concern, but still high. The failure margin for the base plate weld in the tip-over cases is approximately the same as the longitudinal weld in the channel case discussed above. The handling drop has a higher failure margin, with a peak stress of 148 MPa (equal to the yield strength) and a through-wall stress of 90 MPa. The through-wall stress would have to increase by 65 percent to reach the yield limit, and by 540 percent to reach the ultimate strength limit. The handling drop base weld response remains nearly elastic, which puts it in a different stress category than the other locations of interest. There would have to be a significant increase in the load, a significant decrease in cross section thickness, or the introduction of a significant stress concentration factor before the handling drop case would present a challenge to the containment boundary.

The same can be said of the base plate through-thickness stresses, which reach 149 MPa peak and 113 MPa through-wall in the handling drop case. The stress is a bit higher than in the weld, but because the base is a solid plate of material it does not have the potential to be affected by weld imperfections. Through-wall stress would have to increase by over 30 percent to reach through-wall yield, and 430 percent to reach the through-wall ultimate strength limit. Increasing the concrete crush strength did not have a significant effect on this stress. Larger drop heights might increase the stresses. Different assumptions for the initial drop conditions, such as off-centerline drops or drops with a tilted canister, might have a nonlinear effect on the results that changes the overall stress distribution. But apart from considering fundamental changes in the modeled scenario, the base plate stresses would not challenge the containment boundary.

All other combinations of canister location and loading conditions do not present a challenge to the containment boundary. The failure margins discussed here all assume the 148 MPa yield strength and 483 MPa ultimate tensile strength used throughout this study. Changes in the temperature assumptions would affect the failure margins. The consideration of actual (as measured) material strengths might also change the failure margins. Because of the nonlinearity of the models and load cases, scaling of the results to fit alternate stress limits may be reasonable for relatively small adjustments, but major changes in yield strength would necessitate rerunning the models with updated material properties.

6.2 Recommendations for Future Work – Materials Testing or Further FEA

This study identifies the need for high strain rate material data, representative of the stainless steel used in the construction of used nuclear fuel canisters. Of particular interest is the high strain rate behavior of weld material and welded joints. The current models suggest there is a potential to compromise the containment boundary in tip-over scenarios, although this is an artifact of the generic design used and is not indicative of currently licensed systems. With high-strain-rate material testing information it would be possible to incorporate the data into models like the ones used in this study to more accurately determine the response of the containment boundary. It may be that strengthening under high strain rates can handle the stresses without failure, but if that is not the case, it would identify tip-over loading as a serious threat to the containment boundary.

Yield strength, ultimate tensile strength, and elongation at strain rates up to 151 m/m/s are needed to enhance the model's ability to predict failure of the containment boundary. Because the most critical locations are welds, it is recommended that materials testing be focused on welded joints instead of traditional tensile testing of base metal samples. Impact testing of a scale model or bench-scale testing of a welded joint with similar proportions to existing canister lid weld designs would be useful.

A test campaign could be devised to include testing of a welded joint under impact loading accompanied by LS-DYNA modeling. The LS-DYNA material models could be benchmarked against the test data to most accurately replicate the behavior witnessed in testing. Such a test would not have to be costly, and can be simply implemented using two plates welded together, as shown in Figure 6-1. Plate #1 represents the canister shell and Plate #2 represents the lid. This is essentially a two dimensional representation of the welded canister lid. The plate thickness could be relatively thin, but they would have to be restrained against deflecting out of the plane. This testing approach seems plausible and relatively inexpensive, but the main point of this recommendation is to acquire representative high-strain-rate data through testing.

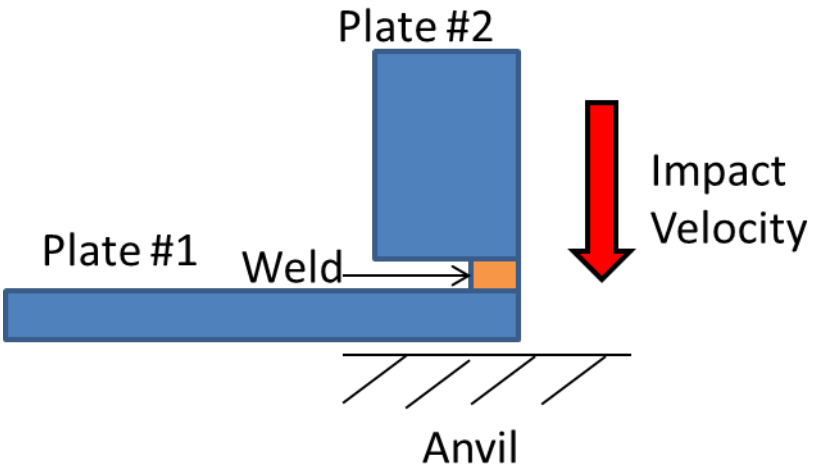

Figure 6-1. Proposed Weld Impact Test Sketch

Another recommendation is to model a specific DSC system in a tip-over scenario to make certain the containment boundary concerns raised in this study remain true. The localized high strain rate loading looks like a fundamental, generic issue, but the influence of design features that were not modeled might offer some unexpected relief. In addition, it would be interesting to assess the effect of gap size between the canister and the cask liner, and what difference the maximum gap condition and minimum gap condition have on the results.

With the baseline and sensitivity results of this study, it is then possible to perform additional modeling to account for degradation of various components. For example, the canister wall or cladding could be thinned due to corrosion or creep. Additional analyses would determine how much degradation could occur before these same events would result in failure of the component. The amount of degradation could then be compared with known rates to determine how long systems and components should last

before their integrity may be compromised by events such as tip-over, drop, or seismic occurrences. Future work will expand to examine the effects on the canister internals, with an emphasis on the fuel assembly and cladding, to determine the impacts on retrievability.

7. REFERENCES

AK Steel Corporation. 2007. 304/304L Product Data Sheet. 304/304L-S-8-01-07. AK Steel Corporation, West Chester, Ohio. Available at http://www.aksteel.com/pdf/markets_products/stainless/austenitic/304_304L_Data_Sheet.pdf.

ASME – American Society of Mechanical Engineers. 2011. *ASME 2010 Boiler and Pressure Vessel Code*, Section II, part D, 2011a Addenda July 1, 2011, American Society of Mechanical Engineers, Three Park Avenue, New York.

CESD – Center for Engineering Strong Motion Data (CESMD). 2011. "Mineral Virginia Earthquake of 23 Aug 2011," http://www.strongmotioncenter.org

DOD – U.S. Department of Defense. 2003. Metallic Materials and Elements for Aerospace Vehicle Structures. MIL-HDBK-5J, U.S. Department of Defense, Washington D.C.

Grecheck ES. 2011. Virginia Electric and Power Company (Dominion), letter to U.S. Nuclear Regulatory Commission, "Virginia Electric and Power Company (Dominion) North Anna Power Station Units 1 and 2 North Anna Independent Spent Fuel Storage Installation Summary Report of August 23, 2011 Earthquake Response and Restart Readiness Determination Plan," Serial No. 11-520, dated September 17, 2011.

Klymyshyn NA, SE Sanborn, HE Adkins, Jr, and BD Hanson. 2013. "Fuel Assembly Shaker Test Simulation," FCRD-UFD-2013-000168/PNNL-22507, Pacific Northwest National Laboratory, Richland, WA.

LSTC- Livermore Software Technology Corporation . 2012. *LS-DYNA® Keyword User's Manual, Volume I*, Version 971 R6.0.0. Livermore Software Technology Corporation, Livermore, California.

LSTC- Livermore Software Technology Corporation. 2012. *LS-DYNA® Keyword User's Manual, Volume II, Material Models*, Version 971 R6.0.0. Livermore Software Technology Corporation, Livermore, California.

Murray YD. 2007. Users Manual for LS-DYNA Concrete Material Model 159. FHWA-HRT-05-062, Federal Highway Administration, Colorado Springs, Colorado.

Murray YD, A Abu-Odeh, and R Bligh. 2006. *Evaluation of LS-DYNA Concrete Material Model 159*. Publication No. FHWA-HRT-05-063, Federal Highway Administration, Colorado Springs, Colorado.

Shirai K, M Wataru, and T Saegusa. 2007. "Experimental Studies of Free-Standing Spent Fuel Storage Cask Subjected to Strong Earthquake." In *Proceedings of the 15th International Symposium on the Packaging and Transportation of Radioactive Materials*, PATRAM 2007.

USGS – United States Geological Survey. 2009. “Shakemap us082311a.” Available athttp://earthquake.usgs.gov/earthquakes/shakemap/global/shake/082311a/

Witte MC, J Hoving, GC Mok, SS Murty, TF Chen, and LE Fischer. 1998. *Summary and Evaluation of Low-velocity Impact Tests of solid Steel Billets onto Concrete Pads*. UCRL-ID-129211, NUREG/CR-6608. Lawrence Livermore National Laboratory, Livermore, California.